NUTRIENT SENSING MECHANISMS IN THE SMALL INTESTINE:

Localisation of taste molecules in mice and humans with and without diabetes

Kate Sutherland, B.Sc. (Hons)

A thesis submitted in fulfilment of the Degree of Doctor of Philosophy

Discipline of Physiology

School of Molecular and Biomedical Sciences

Adelaide University

October 2008

2. IDENTIFICATION AND LOCALISATION OF SWEET TASTE MOLECULES IN THE MOUSE SMALL INTESTINE

2.1 Summary

Background: The molecular mechanisms underlying detection of carbohydrate in the intestinal mucosa are not clear. In contrast GPCR transduction of sweet taste by taste cells of the tongue are relatively well defined. Parallels may exist between chemosensory pathways in the tongue and the gastrointestinal tract as the taste G-protein gustducin ($G\alpha_{gust}$) is specifically expressed in both tissue types. *Aim*s: The aim of these studies was to identify and localise key sweet taste molecules T1R2, T1R3, $G\alpha_{gust}$, $G\gamma_{13}$ and TRPM5 in the mouse intestine to determine if a sweet taste pathway exists for carbohydrates. *Methods:* mRNA extracted from the gastrointestinal mucosa of adult C57 mice was used to confirm expression of taste molecules T1R2, T1R3, $G\alpha_{gust}$ and TRPM5 and transcript levels were quantified using real time RT-PCR. Protein expression was localised in intestinal sections by immunohistochemistry using rabbit polyclonal antibodies for T1R3, $G\alpha_{gust}$ and $G\gamma_{13}$. *Results:* Expression of T1R2, T1R3, $G\alpha_{gust}$ and TRPM5 transcripts was confirmed in the gastrointestinal mucosa. T1R3 was expressed at significantly higher levels in intestinal compared to gastric regions while expression of the sweet taste receptor T1R2 expression was exclusively confined to the small intestine, with highest levels in the jejunum. Solitary epithelial cells in the gastrointestinal mucosa were immunopositive for T1R3, $G\alpha_{gust}$ and $G\gamma_{13}$. These were open-type cells with apical access to the lumen and were most abundant within the proximal jejunum, where they were often most notable within the upper portion of the villus. *Conclusions:* The presence of taste molecules in the mouse small intestine suggest that a transduction pathway similar to that in the tongue operates within the gastrointestinal mucosa. Significant expression of sweet receptors T1R3 and T1R2 in the proximal intestine suggests sweet stimuli are primarily detected at this site. These data indicate that epithelial 'taste' cells

within the proximal small intestine are candidates as primary chemosensory cells of the intestine and as key triggers for carbohydrate-induced feedback control of gastrointestinal function and food intake.

2.2 Introduction

The presence of macronutrients within the lumen of the small intestine is detected by specific sensors within the intestinal wall, which generate positive and negative feedback signals. These signals serve to facilitate digestion and reduce further food intake by regulating pancreatic secretion and gastrointestinal absorption and motility (214, 225, 266). Intestinal carbohydrates for example, stimulate glucose absorption (82), induce satiety (183) and delay gastric emptying (270, 315). Such adjustments serve to optimise nutrient absorption by matching dietary intake of the individual with the absorptive and digestive capacity of the intestinal tract.

The slowing of gastric emptying and reduction in food intake in response to dietary carbohydrate is mediated largely through vagal afferent pathways (270, 382). As carbohydrate absorption is highly efficient and usually completed within the proximal intestine (162) this region is likely to play an important role in the initiation of feedback in response to a normal meal. Indeed, it has been shown in animal and human studies that exposure of only the proximal half of the small intestine to nutrient results in a greater delay in gastric emptying than when nutrients are delivered to only the distal half of the small intestine (188, 216, 360, 361). The proximal intestine therefore appears to be an important site for the initiation of this feedback regulation of gastric motility and satiety, however, the cellular and molecular mechanisms which govern this feedback control are not well understood.

Vagal afferent fibres that innervate the intestine respond to nutrients by increasing afferent discharge, such as in the presence of luminal glucose (209, 315, 381). Studies using axonally transported dyes injected into the nodose ganglion have allowed visualisation of vagal afferents in the intestine, and have shown that

fibres innervate individual villi within the duodenum (16) and are most densely concentrated in the duodenum and thereafter decrease in frequency towards the colon (95, 356). These anatomical studies also established that vagal afferent endings terminate in the lamina propria below the epithelial layer and do not penetrate the epithelial barrier to directly sample luminal contents. Detection of ingested nutrients by vagal afferents must therefore take place indirectly.

Two anatomical models for the activation of vagal afferents by luminal glucose have been proposed, either direct or indirect activation (113). In the direct detection model glucose is transported from the lumen via specific transporters in the apical and basolateral membranes of enterocytes (256). Glucose is then released into the sub-epithelial interstitial space, where vagal afferent terminals have direct access to glucose molecules. Accordingly, vagal afferent terminals in this model must possess molecular machinery for direct detection of glucose.

In contrast, indirect detection of glucose by vagal afferents proposes that luminal glucose is detected prior to absorption by an epithelial 'sense' cell, which responds by releasing a neuroactive substance from the basolateral surface that directly stimulates adjacent afferent fibres. Gut enteroendocrine cells are candidate cell types ideally suited to the role of sense cells and are proposed to be the primary chemosensors for nutrients in the small intestine (266). Enteroendocrine cells have apical microvilli directly exposed to the luminal chemicals and basolateral secretory vesicles for release of various hormones, many of which are neuroactive (174, 282). In this indirect model the molecular machinery for glucose detection is located in the apical epithelium of the sense cell.

In order to understand peripheral mechanisms of glucose detection in the gut it is useful to make comparisons to conceptually related chemosensory systems, such as taste recognition in the lingual epithelium (100, 113). Taste receptor cells are specialised neuroepithelial cells found clustered in taste buds

on the surface of the tongue. Apical microvilli on individual taste cells are exposed to the oral cavity while sensory nerves are associated with the basolateral surface of the taste bud. Recognition of sapid compounds through the apical membrane results in membrane depolarisation of taste cells leading to neurotransmitter release, activation of afferent fibres and subsequent transmission of taste signals to centres in the brain (127, 191).

Molecular mechanisms involved in sweet taste on the tongue have recently been revealed. Both natural and artificial sugars are detected by members of the T1R family of GPCR, specifically a heterodimer of T1R2 and T1R3 (185, 237). Signal transduction molecules involved in sweet taste include the taste cell specific G-protein components $G\alpha_{gust}$, and $G\gamma_{13}$, and ion channel TRPM5 (152, 364, 377).

Recent studies in gastrointestinal tissues have provided evidence that the intestinal mucosa possesses similar molecular machinery for sweet taste to that of the lingual mucosa. First evidence was provided in northern blot studies which showed specific hybridisation of taste molecules $G\gamma_{13}$ and TRPM5 in both lingual and intestinal tissues (152, 257). T1R2, T1R3 and $G\alpha_{gust}$ transcripts have since been detected in the rodent intestine and in an enteroendocrine cell line using real time, reverse transcriptase-polymerase chain reaction (RT-PCR) (81, 137, 366). $G\alpha_{gust}$ has also been identified in individual epithelial cells within the rat duodenum (137) suggesting the presence of 'taste' cells within the intestinal epithelium.

Despite emerging data on the presence of sweet taste molecules in the intestine, information on specific expression, location and functions are lacking. Confirmation of this expression and localisation to individual cells (whether within cells of the epithelium or on sub-epithelial nerve fibres) throughout the small intestinal tract would reveal molecular and anatomical details (direct or indirect model) of this putative carbohydrate detection mechanism. Moreover, such knowledge will add considerably to understanding on whether carbohydrates are detected in the mucosa and initiate regulatory reflexes (such as the inhibition of gastric

emptying and food intake) via sweet taste mechanisms. This work forms the basis for studies investigating expression of taste transduction molecules in relation to that of mediators of carbohydrate-induced intestinal feedback.

2.3 Aim

To identify and localise the expression of key sweet taste molecules in the mouse small intestine.

2.4 Specific hypotheses

1. Sweet taste molecules T1R2, T1R3, $G\alpha_{gust}$, $G\gamma_{13}$ and TRPM5 are specifically expressed in the mucosa of the mouse small intestine.

2. Sweet taste molecules are preferentially expressed in the proximal half of the small intestine where carbohydrate-sensing and absorption primarily take place.

3. Sweet taste molecules in the small intestine can be localised to individual cells within the villous epithelium.

2.5 Materials and methods

All experiments were performed using adult male C57BL/6 mice aged 7-10 weeks, housed conventionally with free access to water and a standard laboratory rodent diet. All studies were performed in accordance with the Australian code of practice for the care and use of animals for scientific purposes and with the

approval of the Animal Ethics Committees of the Institute of Medical & Veterinary Science (Adelaide, Australia) and the University of Adelaide.

2.5.1 Immunohistochemistry

2.5.1.1 Animal preparation

Mice were anesthetized by intraperitoneal injection of sodium pentobarbitone (60mg/kg). Once mice were assessed to be no longer responsive to a standard hind limb pinch test the thoracic cavity was opened to expose the pericardium. A single injection of 0.2 ml heparin was given into the left ventricle to minimise clotting. A blunt needle (21 gauge) connected to a perfusion system was then inserted into the left ventricle via the apex and the vena cava cut to allow blood and perfusate to drain from the body. Warm saline was then perfused through the circulatory system at a rate of 20 ml/min until perfusate was clear of blood. This was immediately followed by perfusion of cold 4% paraformaldehyde in 0.1M phosphate-buffered saline (PBS), pH 7.4, 50 ml to fix tissues. The tongue and the entire length of the small intestine were excised for post-fixation processing.

2.5.1.2 Tissue preparation and sectioning

The small intestine was cut longitudinally along the cephalocaudal axis, pinned flat and flushed with fresh fixative. The tongue and small intestine were postfixed in 4% paraformaldehyde-PBS for 2 - 4 hrs at room temperature. Fixative was then removed from the tissue with three washes of PBS after which the tissue was cryoprotected in 30% sucrose/PBS overnight at 4ºC. Tissues were then embedded in O.C.T compound

(Tissue-Tek) in cryomoulds and rapidly frozen in liquid nitrogen. All tissue blocks were stored in foil at -80ºC until needed.

Frozen sections of embedded tissue were cut at 14 µm on a cryostat (CRYOCUT 1800 Reichert-Jung). The tongue was sectioned longitudinally from base to tip to allow visualisation of the posterior circumvallate papillae and scattered fungiform papillae within the same section. Intestinal sections were cut transversely to reveal all layers of the intestine within the same plane. Sections were thaw mounted directly onto gelatine coated glass slides, and slides used immediately, or stored at -20ºC for no more than a few days. Small intestinal tissue from six mice was used in this experiment.

2.5.1.3 Antibodies

Commercial antibodies that recognised sweet taste molecules were unavailable or of insufficient quality at the time of study. As an alternative, polyclonal primary antibodies raised against mouse protein sequences for T1R3, $G\alpha_{gust}$, $G\gamma13$ and TRPM5 were obtained from Professor Robert Margolskee (Department of Neuroscience, Mount Sinai School of Medicine, New York) via collaboration. Specific information concerning the primary antibodies used in these studies is detailed below in Table 2.5.1.

Table 2.5.1 Primary antibody information.

Detected protein	Antibody	Corresponding peptide sequence	Working dilution
T1R3	rabbit, polyclonal	(C)HEGLVPQHDTSGQQLGK-COOH	1:400
$G\alpha_{gust}$	rabbit, polyclonal	(C)YVNPRSREDQQLLLS-COOH	1:500
$G\gamma13$	rabbit, polyclonal	(C)FLNPDLMKNNPWV	1:500
TRPM5	rabbit, polyclonal	(C)RKEAQHKRQHLERDLPDPLDQK	1:400

2.5.1.4 Indirect immunofluorescence protocol

Slides were air dried at room temperature for 15 min and sections encircled by a waterproof barrier (pap pen). Sections were washed three times for 10 min in PBS containing Triton X-100 (PBS + 0.2% Triton X-100, Sigma-Aldrich, pH 7.4, PBS-T) to facilitate antibody penetration. A normal goat serum blocking solution was prepared of 2% goat serum (for blocking), 1% bovine serum albumin (BSA) (stabliser), 0.1% cold fish skin gelatin (blocking), 0.1% Triton X-100 (penetration enhancer), 0.05% Tween 20 (detergent and surface tension reducer) and 0.05% sodium azide (preservative) in PBS. Sections were incubated with blocking solution for 1 hr at room temperature. Primary antibodies were diluted to their appropriate working concentration (refer to Table 2.5.1) in blocking solution and sections incubated in the primary antibody solution at 4ºC overnight (approximately 18 hrs). Sections were then rinsed three times with PBST to remove any remaining unbound primary antibody. Antibody label was visualised with a goat anti-rabbit Alexa Fluor® 546 secondary antibody (Molecular probes, Eugene, OR, USA). The secondary antibody was applied at a 1:200 dilution in PBST for 1 hr at room temperature. Excess secondary antibody was removed by three PBST washes then sections were mounted in ProLong® Antifade reagent (Molecular probes, Eugene, OR, USA) and coverslipped. Slides were allowed to dry before the edges of the coverslip were sealed with nail varnish.

2.5.1.5 Immunohistochemical controls

Tongue sections were included as positive controls to test for specificity of taste molecule antibodies, while sections lacking the primary IgG, served as negative controls, to assess non-specific binding of the secondary antibody.

2.5.1.6 Visualisation

Sections representing duodenum, jejunum and ileum from each animal were examined and epifluorescent images obtained on an epifluorescence microscope (BX-51,Olympus, Australia) equipped with multiple excitation filters. Images were acquired on a monochrome charge-coupled device digital camera system (Photometrics CoolSNAP*fx*, Roper Scientific, Tuscon AZ). Fluorescence images were imported unmodified into V^{++} Precision Digital Imaging System software (version 4.0, Digital Optics, Auckland, New Zealand), pseudo-coloured and merged for composite images; luminance intensity was not adjusted.

2.5.2 Reverse-transcriptase polymerase chain reaction (RT-PCR)

2.5.2.1 Tissue collection

Mice were humanely killed by asphyxiation with CO_2 and all tissues dissected in ice-cold sterile saline in an RNAse-free environment using sterile equipment. The tongue was quickly excised at the base, the circumvallate papillae identified and the lingual epithelium distal to the papillae dissected away from the adjoining muscle tissue. A small segment of the outer cortex of the kidney was also obtained as negative control tissue. Tissues were immediately submerged in approximately 10x their volume of the RNA stabilisation reagent, RNAlater® (Qiagen, Australia). Representative segments of the distal esophagus, gastric fundus, body and antrum were excised and the outer muscle layers peeled off and discarded. The remaining epithelial layers were transferred into RNAlater. All tissues collected in RNAlater were stored overnight at 4°C to allow thorough penetration into tissue before being transferred to -20°C for longer-term storage. Duodenal, jejunal and ileal segments of the small intestine were excised, opened longitudinally along the anti-mesenteric border and pinned out flat in a dissection tray. A scalpel blade was used to scrape

the mucosal layer off the outer muscle layers. As storage of mucosal tissue in RNAlater made subsequent retrieval difficult, mucosal tissue was immediately snap frozen in liquid nitrogen and used immediately or stored at -80°C as necessary.

2.5.2.2 RNA extraction

Total RNA was extracted from all tissues using a commercial RNA extraction kit, the RNeasy Mini Kit (Qiagen), according to manufacturer's instructions for animal tissues. Tissue was placed in a sterile glass mortar, which was snap frozen in liquid nitrogen to prevent tissue thawing, and was ground into a fine powder using a glass pestle. 600 µl of guanidine-thiocyanate-containing stabilisation and lysis buffer (Buffer RLT) including 140 mM β-Mercaptoethanol (Sigma-Aldrich, Sydney, Australia) was then added to the tissue powder. A sterile pasteur pipette was used to transfer the lysate directly onto a QIAshredder spin column placed in a 2 ml collection tube (Qiagen) for homogenisation by centrifugation at 12,000 rpm for 2 min. The QIAshredder columns were discarded and the collection tubes containing the homogenate were capped and centrifuged for a further three minutes after which the supernatant was carefully removed, taking care not to disturb the pellet. 600 µl of 70% ethanol was added and mixed with the cleared lysate by pipette. Total RNA was bound to the silica-based membrane of an RNeasy spin column by a 15 sec centrifuge step (12,000 rpm) and the flow through was discarded. A first wash step to remove contaminants from the membrane was performed by centrifugation of 350 µl of Buffer RW1 through the RNeasy spin column, with the flow through discarded. An on-column DNase digestion was then performed by adding 80 µl of DNase 1 in Buffer RDD (RNase-Free DNase Set, Qiagen) directly to the spin column membrane followed by a 15 min incubation at room temperature. DNase and contaminants were further removed by wash steps with 350 µl of Buffer RW1 and two washes of 500 µl Buffer RPE at 12,000 rpm in the centrifuge. To thoroughly remove any Buffer RPE and traces of flow-through the column was transferred to a new collection tube and centrifuged at 12,000 rpm for 1 min. Once dried, the spin-column was inserted into a new tube in which to

collect RNA. RNA was eluted from the spin-column by applying 30 µl of RNase-free water directly onto the silica membrane and centrifuging for 1 min at low speed. A second application of 30 µl of RNase-free water was passed through the column in samples where a high RNA yield was expected. The concentration and purity of the resulting RNA sample was then assessed by UV spectroscopy. A 100 µl sample was prepared for quantification with purified RNA diluted 1:50 in TE buffer (1M Tris Cl, 0.5M EDTA, ph 8.0, Sigma). TE buffer (100 µl) was placed into a sterile cuvette and used to blank the spectrophotometer (Biorad); the blanking solution was removed and replaced with the sample containing RNA. RNA quantification was performed by measuring absorbance at 260 nm (A_{260}) in triplicate and the purity of the sample was assessedd by the A_{260}/A_{280} ratio. A ratio of 1.8 - 2.1 indicates highly purified RNA and in all samples used the A_{260}/A_{280} ratio fell within this range. The purified template RNA was stored in aliquots of 5 µl at -80°C until needed.

2.5.2.3 Primers

Expression of T1R2, T1R3, $G\alpha_{gust}$ and TRPM5 was measured in gastrointestinal tissue using RT-PCR. Primers sets for each gene were purchased commercially as validated QuantiTect primer assays (Qiagen). QuantiTect primer assays consist of optimised forward and reverse primers that are derived from sequences contained in the NCBI Reference Sequence database (www.ncbi.nlm.nih.gov/RefSeq) and generally do not to detect contaminating genomic DNA. QuantiTect primer assays are validated for use in real-time RT-PCR assays using SYBR® Green detection in any real time cycler. For T1R3, additional primers were designed using Primer 3.0 software (Applied Biosystems, Foster City, CA) based on the gene sequence obtained from the NCBI nucleotide database. One primer of the pair was designed to span an exon-exon boundary as determined from exon information in the Ensembl gene database (www.ensembl.org) in order to avoid co-amplification of any contaminating genomic DNA in the sample.

Specific information on all primers used can be found in Table 2.5.2. Additional QuantiTect primer assays for β-actin and 18s rRNA used for control and reference reactions were included.

Table 2.5.2 Primers for amplification of mouse taste molecule genes and controls in RT-PCR reactions.

Gene	Entrez gene ID	Accession no.	Length of transcript (bp)	Primer information	Amplicon length (bp)
T1R2 (Tas1r2)	83770	NM_031873	3060	QT00142639	137
T1R3 (Tas1r3)	83771	NM_031872	3514	QT00309890	110
				Forward (5' to3'): caaaacccagacgacatcg	137
				Reverse (5' to 3'): catgccaggaaccgagac	
$G\alpha_{gust}$ (Gnat3)	346562	XM_144196	1174	QT00049784	105
Trpm5	56843	NM_020277	4032	QT00161602	183
β-actin (Actb)	11461	NM_007393	1892	QT00095242	149
18s RNA (Rn18S)	19791	X00686	1869	QT01036875	149

QT, QuantiTect primer assay, catalogue number (Qiagen)

The specific sequences of the commercially purchased primers are not available but schematics given by the manufacturer show the approximate locations of the amplified regions for each target sequence (Figure 2.5.1).

Figure 2.5.1 Approximate location of amplicon sequences in target mouse genes detected by QuantiTect Primer Assays.

Validated forward and reverse primers for gene sequences contained in the NCBI Reference Sequence database are commercially available as QuantiTect Primer Assays from Qiagen. Specific sequence information of the primers and corresponding amplicons are not available, however, schematic representations of the approximate region of the target genes amplified in PCR reactions are shown for T1R2 (A), T1R3 (B), $G\alpha_{gust}$ (C), TrpM5 (D), β-actin (E) and 18S RNA (F). Primer assays are optimised and guaranteed for use in real time RT-PCR reactions in any real-time cycler with QuantiTect SYBR green kits.

All primer sets produced PCR products of no more than 200 base pairs (bp) - standard for real time PCR reactions due to the higher amplification efficiency of shorter amplicons (37). All primer sets had an estimated melting temperature (T_m) of 60°C, in accord with published evidence of optimal RT-PCR reaction at 60°C (37). This allowed identical annealing temperatures (usually 5°C below the T_m) to be used for all PCR reactions. All lyophilized primers were reconstituted in sterile TE buffer and stored in aliquots at -20°C.

2.5.2.4 RT-PCR protocol

Reverse transcription and PCR were performed using a one-step RT-PCR kit (Qiagen). All reaction components including template RNA, primer solutions, RNase-free water and one-step RT-PCR kit reagents were kept on ice and thoroughly mixed by pipette upon thawing to avoid localised differences in salt concentrations. All reactions were prepared on ice inside a PCR hood equipped with a UV light source; all surfaces and equipment were decontaminated using the RNase decontamination solution, RNase*Zap*™ (Ambion) prior to, and after use.

A master-mix was prepared according to the manufacturer's specifications for 50 µl PCR reaction volumes. For each PCR reaction 10 µl of RNase-free water, 10 µl of 5x QIAGEN OneStep RT-PCR Buffer, 2 µl dNTP Mix (containing 10 mM of each dNTP), 2 µl QIAGEN OneStep RT-PCR Enzyme Mix and 1 µl of RNase inhibitor (Ambion) was combined in a sterile eppendorf tube and gently mixed. 25 µl of the prepared master-mix was then added to a 0.2 ml clear thin walled PCR tube (Axygen). Primers were added to the PCR tubes in amounts corresponding to a final concentration of 0.6 µM in the reaction volume, either 5 µl of 10x stock solution of QuantiTect Primer Assay, or 10 µl each of 3 µM forward and reverse primers. RNase-free water was used to dilute template RNA to 50 ng and 5 µl of template, equating to a final concentration of 5 ng, was added to each reaction. In PCR reactions containing QuantiTect Primer Assays an additional 15 µl of RNase-free water was added to make up the 50 µl volume.

RT-PCR reactions were performed using an alpha unit block for PTC DNA engine systems (MJ Research, Waltham, MA, USA) attached to a PTC-200 Peltier thermal cycler (MJ Research). The amplification programme applied to the thermal cycler started with reverse transcription at 50°C for 30 min followed by an initial PCR activation step at 95°C for 15 min. This heating step activates the HotStarTaq DNA polymerase while inactivating Omniscript and Sensiscript Reverse Transcriptases and denaturing the cDNA template. PCR cycling consisted of three 1 min steps; denaturation 94°C, annealing 55°C and extension 72°C, which was repeated 40 times followed by a final extension step at 72°C for 10 minutes. PCR tubes were kept on ice and placed in the thermal cycler only when the initial temperature of 50°C was reached, to ensure that reverse transcription of template RNA was immediate and specific. Amplified PCR products were stored at -20°C.

2.5.2.5 RT-PCR controls

Positive and negative tissue controls were included in initial RT-PCR reactions. RNA from tongue tissue was used as a positive control for specific expression of taste molecule genes, while RNA from kidney tissue was used correspondingly as a negative control for taste molecule gene expression. Internal controls for RT-PCR were performed with primers for the housekeeping gene β-actin, which is abundantly expressed in the majority of cell and tissue types. Signals from the internal control reactions should be observed in all RT-PCR assays to confirm the viability of the amplification process. A no template control (NT) was also included in all PCR assays to detect contamination of samples; this included all reaction components except the template RNA, which was replaced with 5µL of nuclease-free water. Any products resulting in these reaction tubes are directly attributable to contamination by nucleic acids.

Primer sets used in RT-PCR assays were designed to avoid contamination by genomic DNA (gDNA) by at least one primer spanning an intron across an exon-exon boundary. This prevented binding of the primer to

gDNA template (unless pseudogenes with identical or near identical nucleotide sequences were present). The on-column Qiagen RNA extraction protocol reports to purify RNA virtually free of DNA, however an additional on-column RNase-free DNase 1 digestion step was performed during the RNA extraction on all samples, with the DNase removed in subsequent wash steps. It has been reported, however, that there are wide variations in the RNA content of purified nucleic acid both before and after DNase treatments (38) with some preparations containing virtually pure RNA while in others RNA constitutes only 50-80% of the purified sample. The resulting RNA content of nucleic acid samples were DNase treatment-, tissue origin- and operator-independent (38). For this reason false-positive signals resulting from gDNA amplification were controlled in no reverse transcription reactions (-RT). In this type of control, reactions are prepared in identical manner to sample reactions except they do not undergo the reverse transcription step and no template will be available for PCR amplification unless there is contaminating DNA in the sample. In the one-step RT-PCR method used, –RT controls were kept on ice during the initial reverse transcription step and added to the thermal cycler only once the temperature had reached 94°C for initial PCR activation of HotStarTaq DNA polymerase. The activated DNA polymerase also performs the function of inactivating the reverse transcriptase enzymes ensuring temporal separation of reverse transcription and PCR.

2.5.2.6 Gel electrophoresis

Amplified products resulting from RT-PCR were resolved by gel electrophoresis using pre-made 20-well 3% agarose/TBE buffered gels containing ethidium bromide (Bio-Rad) in a gel tank containing TBE buffer. 5 µl of product was combined with 2 µl of nucleic acid sample loading buffer (Bio-Rad) and transferred by pipette into the wells of the gel. A 100 bp DNA ladder molecular weight marker was run on every gel to confirm the expected product size. Gel electrophoresis was completed at 70 mV and amplification products were visualised after separation inside a gel dock system under UV light and imaged using a CCD camera and UV photometer software.

2.5.2.7 Quantification method for real time RT-PCR

The simplest detection technique for monitoring the amount of RT-PCR product is the use of double strand DNA binding agents. SYBR Green I fluorescence dye exhibits little fluorescence when it is unbound in solution but binds specifically to the minor groove of double-stranded DNA molecules during the elongation step of every PCR cycle. Fluorescence levels measured at the end of each PCR cycle therefore increase in proportion with the amount of amplified product. The PCR cycle number is plotted against the fluorescence level as a PCR amplification curve (Figure 2.5.2). The threshold cycle (C_T) is the PCR cycle at which the fluorescence level crosses a fixed threshold line, which is set in the early exponential phase when fluorescence first increases above baseline. The C_T can be used to calculate the starting amount of template in each sample. Gene expression can be quantified from real time RT-PCR by two alternate strategies. *Absolute quantification* determines the copy number of mRNA transcripts using an external calibration curve of known copy numbers. However in the majority of situations *relative quantification* where amount of target gene is expressed as a ratio of a reference gene is appropriate. Various mathematical models have been developed to calculate the expression level of a target gene relative to a reference gene using their respective C_T values to calculate changes in gene expression by fold difference between experimental and calibrator samples. The simplest method of performing relative quantification is by calculating the theoretical value R_0. This is based on a simple formula, which simulates a PCR reaction until it reaches plateau and on which mathematical models of relative quantification is based.

$$X_n = X_0 X (1 + E)^n \qquad [1]$$

Here X_n represents the amount of template at cycle n, X_0 the starting template amount and E the amplification efficiency. During real time PCR the amount of fluorescence is proportional to levels of accumulated PCR product so this equation may be rewritten in terms of fluorescence (R).

$$R_0 = R_{ct} X (1 + E)^{-ct} \quad [2]$$

Here R_0, the starting fluorescence, is proportional to the starting template quantity. R_{Ct} is the fluorescence at the C_T, which is the fluorescence threshold set by the user and E is the efficiency of the PCR reaction (100% efficiency of a PCR reaction indicates that the amount of PCR product doubles at each cycle). R_0 can be obtained for samples containing target and reference genes and expressed as ratio $R_{0\ target} / R_{0\ reference}$ to obtain normalised relative quantification data.

NOTE:
These figures are included on page 61 of the print copy of the thesis held in the University of Adelaide Library.

Images from QuantiTect SYBR Green RT-PCR handbook (Qiagen)

Figure 2.5.2 Real time PCR data acquisition and verification of product specificity.
Real-time PCR amplification curves (A) present the level of fluorescence emitted at each reaction cycle. Signal is first detected during the early exponential phase before exponentially increasing as product accumulates (log-linear phase). Plateau is reached in later cycles due to signal saturation. Starting and amplified template amounts are directly proportional during the exponential phase where a threshold level is set; threshold cycle (C_T). In the example two samples (A and B) are amplified, sample A contains a higher amount of starting template than B as the C_T is reached earlier. Melting curve analysis (B) is used to verify the identity and specificity of amplified PCR products. The melt curve, obtained subsequent to amplification by recording fluorescence levels over a gradient temperature increase, represents the temperature dependence of the fluorescence. Fluorescence is high at low temperatures when products are double stranded and low at high temperatures when products are denatured. The product's T_m is the temperature at which the sharpest decrease in signal occurs and corresponds to the peak of the curve in the negative first-derivative. Non-specific products differ in length and therefore their melting temperatures produce different peaks. In the example sample A yields only one peak as a result of amplification of one specific product, whereas sample B exhibits a peak from the specific product and another peak at a lower temperature indicative of amplification of primer dimers.

2.5.2.8 Real time RT-PCR protocol

RT and PCR were performed using a QuantiTect® SYBR® Green RT-PCR kit (Qiagen) using a one-step RT-PCR protocol. The kit comprises 2x QuantiTect SYBR Green RT-PCR master-mix (containing DNA polymerase), SYBR Green 1 and ROX fluorescent dyes (ROX = a passive reference dye for normalisation of fluorescent signal), RT-PCR buffer, dNTP Mix and QuantiTect RT Mix containing Omniscript® and Sensiscript® reverse transcriptases. A master-mix was prepared according to the manufacture's instructions for a 50 µl reaction volume by thoroughly mixing 25 µl of 2x QuantiTect SYBR Green with 0.5 µl of QuantiTect RT mix per PCR reaction. Reactions were prepared on ice in the same manner and RNase-free conditions as for end-point RT-PCR. For each reaction 25 µl of total master mix was added to MJ White PCR tubes (MJ Research). Primer details are shown in section 2.5.2.3 and Table 2.5.1; these were used according to protocols for QuantiTect Primer Assays, which provide specific and sensitive quantification. 5 µl of 10x QuantiTect Primer Assay (or for the additional T1R3 primer, 10 µl each of 3 µM forward and reverse primer), were added to the reaction tube to provide a final concentration of 0.6 µM. Template RNA was diluted in RNase-free water to a quantity of 50 ng in 5 µl and added to the each sample tube. Reaction volumes were made up to 50 µl with RNase-free water (15 µl for reactions using QuantiTect Primer Assays). NT control reactions were included by substituting RNA with nuclease-free water.

RT-PCR reactions were performed using a Chromo4 (MJ Research) real-time instrument attached to a PTC-200 Peltier thermal cycler (MJ Research) and data acquired with Opticon Monitor 3.00 software (MJ Research). The real-time cycler was programmed as follows: Reverse transcription 50°C for 30 min, initial PCR activation step 95°C for 15 min (this heating step activates the DNA polymerase, deactivates the reverse transcriptases and denatures the cDNA template), 3-step PCR cycling of denaturing 94°C for 15 sec, annealing 55°C for 30 sec, extension 72°C for 30 sec, which was repeated 40 times with fluorescence data collected at the end of each cycle. A melt curve analysis was included after the amplification

programme was completed to verify the specificity and identity of the resulting RT-PCR products (Figure 2.5.2b). The melt curve programme was applied by increasing the temperature from 65°C to 95°C in 1°C increments held for 15 sec with the fluorescence level read from the plate at each stage. Fluorescence was then plotted against temperature to create the melt curve.

Each target and reference assay was performed in triplicate with RNA samples from each of three animals and in separate experiments.

2.5.2.9 Real time RT-PCR data and statistical analysis

The threshold line in all experiments was set at 0.05, which corresponded to the early exponential phase of product amplification for all assays. The C_T values of all replicates of targets and references were calculated by the Opticon Monitor software and copied into a spreadsheet where the difference in cycle number ($\triangle C_T$) between targets and references were used to individually quantify relative gene expression differences between a single control and sample. Each target and reference reaction was run in triplicate for each of the three animals with no pooling of RNA samples.

For real time analysis purposes, within each animal each replicate was not averaged before calculation but treated as independent samples, with each replicate of the target assay referenced to each of the reference replicates to obtain a total of nine $R_{0\ target}$ / $R_{0\ reference}$ values for each gene target per sample from each animal. These nine numbers were then averaged for each animal to produce the final total for that animal and the mean of these 3 final numbers from each of the three animals is presented in the final data. This was done to counteract experimental variation between experimental replicates within each animal. As each tube is likely to vary slightly but with potentially wider discrepancies, instead taking the overall average of three, referencing each replicate to each target provides more precision.

Relative RNA levels were expressed as mean ± standard error of the mean (SEM) and a one-way ANOVA with Tukey's post hoc test was performed to compare expression levels of target genes between regions of the gastrointestinal tract. A p value of < 0.05 was considered significant.

2.6 Results

2.6.1 Immunohistochemistry

Validation of antibodies for taste proteins in tongue tissue

The antibodies used in this study were initially tested in tongue sections to confirm their specificity for mouse taste molecule proteins based on previously published immunolabelling with these antibodies in the tongue (65, 152, 257, 369) and to optimise immunolabelling quality prior to assays in test tissues. Antibodies that recognised T1R3, $G\alpha_{gust}$, $G\gamma13$ and TRPM5 only labelled taste cells within fungiform, foliate and circumvallate papillae in the lingual epithelium. The distribution of immunopositive cells for each antibody, however, did display differences in expression within each papillae type.

Antibodies that recognised G-protein components, $G\gamma13$ and $G\alpha_{gust}$ displayed similar patterns of immunoreactivity across the tongue's surface. $G\gamma13$ label was confined to the cytoplasm of taste cells located within fungiform, foliate and circumvallate papillae, and was apparent in the majority of taste cells (Figure 2.6.1.1). Similarly the rabbit polyclonal $G\alpha_{gust}$ antibody robustly labelled the cytoplasm of taste cells within taste buds of each papillae type. Most taste cells within sections containing fungiform papillae (Figure

2.6.1.2) were immunopostiive for $G\alpha_{gust}$ as were the taste cells within foliate and fungiform papillae (Figure 2.6.1.3). Overall $G\alpha_{gust}$ immunoreactivity was present in a greater proportion of taste cells than label for the other taste molecule proteins and labelled with intense immunofluorescence and high signal to background ratio and was highly reproducible in all sections tested.

Specificity of the rabbit polyclonal T1R3 receptor antibody was confirmed by labelling within the cytoplasm of lingual taste cells. In fungiform papillae (which contain only a single-taste bud) an occasional taste cell was found to be immunopositive (Figure 2.6.1.4 A,B) although in the majority of these cases the intensity of labelling appeared marginal to the eye. However, in contrast to sections incubated with $G\gamma13$ and $G\alpha_{gust}$, the majority of fungiform taste buds did not contain any identifiable immunopositive cells (Figure 2.6.1.4 C,D). This did not appear to reflect the quality or viability of the antibody but localised expression of T1R3, as the taste buds of the posterior tongue contained robust immunoreactivity (Figure 2.6.1.5). The taste buds of the foliate (Figure 2.6.1.5 A,B) and circumvallate papillae (C,D) contained individual taste cells displaying intense cytoplasmic immunoreactivity. Not every cell within these taste buds appeared to be T1R3 immunopositive but at least one labelled cell could be observed in each visible taste bud.

Immunohistochemistry for TRPM5 on the whole did not produce results consistent with the labelling patterns of the other taste molecule proteins (Figure 2.6.1.6). The primary antibody was tested over a range of concentrations and immunohistochemical protocols in tissue from multiple mice. No specific labelling of taste cells in fungiform papillae could be consistently observed (Figure 2.6.1.6 B) with only one or two immunopositive taste cells identified throughout all labelled sections (Figure 2.6.1.6 A). Similar results were obtained in circumvallate and foliate taste buds, with taste buds on occasion displaying immunolabelling at levels above background (Figure 2.6.1.6 C). However, this labelling was at an order of intensity lower than that for other taste targets, and most sections were immunonegative (Figure 2.6.1.6 D). In serial sections, where positive labelling for T1R3, $G\gamma13$ and $G\alpha_{gust}$ was identified in taste cells, the same taste cells did not

label for TRPM5 (Figure 2.6.1.6 D). This observation suggests that the antibody is not able to effectively label TRPM5 protein in frozen sections. The suboptimal performance of this antibody in positive control tissue therefore made it unsuitable for assessment in test tissues.

Negative controls, where the primary antibody was omitted, were included in all assays and did not show immunolabelling in any taste cells. This confirmed that immunofluorescence was due to the specific binding of the primary antibody to taste cells targets. The antibodies had also been previously validated as being specific for each taste protein in blocking experiments using the corresponding control peptide for each antibody.

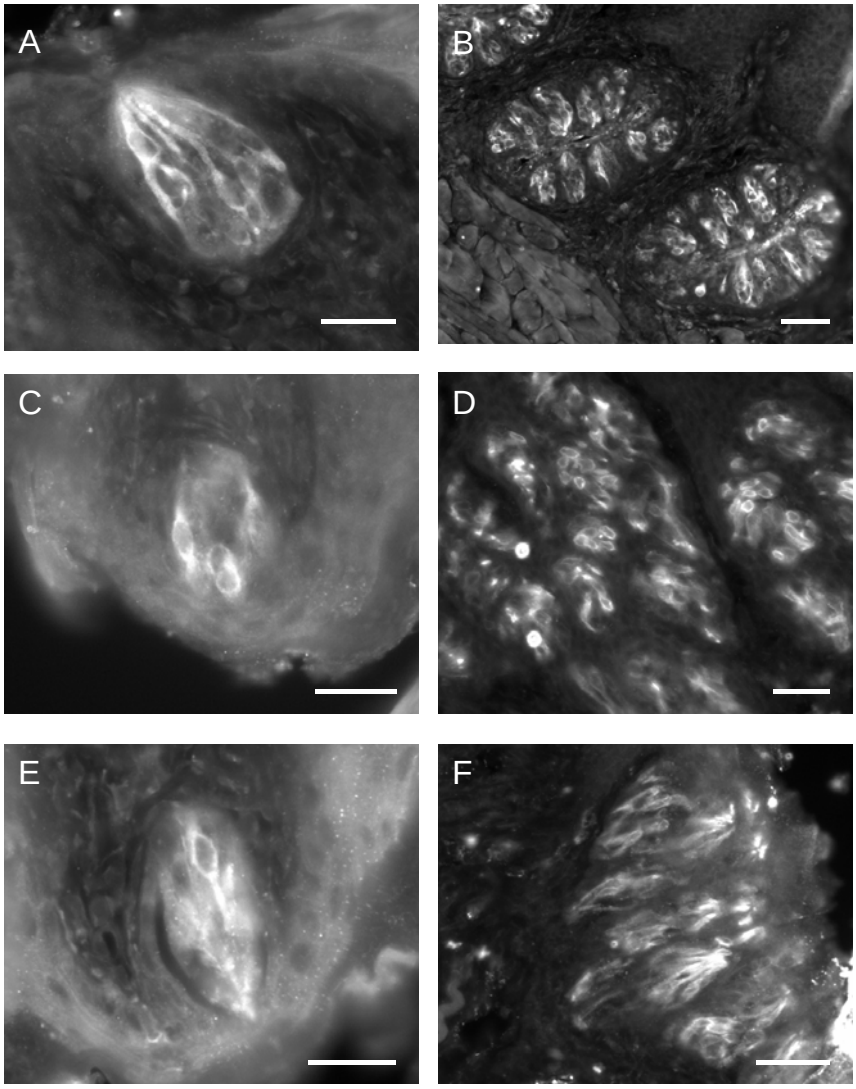

Figure 2.6.1.1 Gγ13 immunoreactivity in taste cells of the mouse tongue.
Immunohistochemistry using a polyclonal antibody against Gustducin G-protein complex subunit Gγ13 produced immunofluorescence specific to taste cells in the lingual epithelium. In fungiform papillae, immunoreactivity was specificly found within the cytoplasm of taste cells (A, C, E). Gγ13 immunopositive taste cells were also found within the multiple taste buds lining the foliate (B) and circumvallate (D, F) papillae. Most taste cells within these taste buds were immunopositive, as shown in a cross-section of circumvallate taste buds (D) where immunofluorescence surrounds the unlabeled nuclei of the taste cells. Scale bars = 50 µm (A, C, E, F) and 100 µm (B, D).

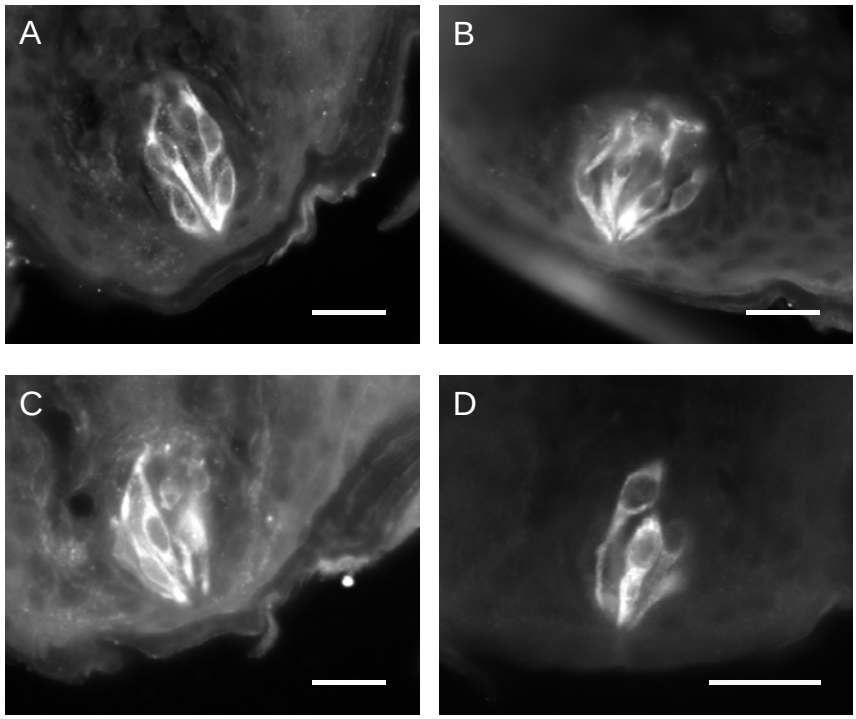

Figure 2.6.1.2 Gα_{gust} immunoreactivity in taste cells of fungiform papillae of the mouse tongue. The specificity of the polyclonal Gα_{gust} antibody for taste cells was confirmed in the taste buds of fungiform papillae. The single taste buds of this papillae type contain immunopositive taste cells displaying robust fluorescence homogenous throughout the cytoplasm (A-D). Most visible taste cells within the section of the taste bud appear to be immunopositive. Gα_{gust} expressing taste cells were found in all the fungiform papillae of the anterior papillae. Scale bars = 50 µm.

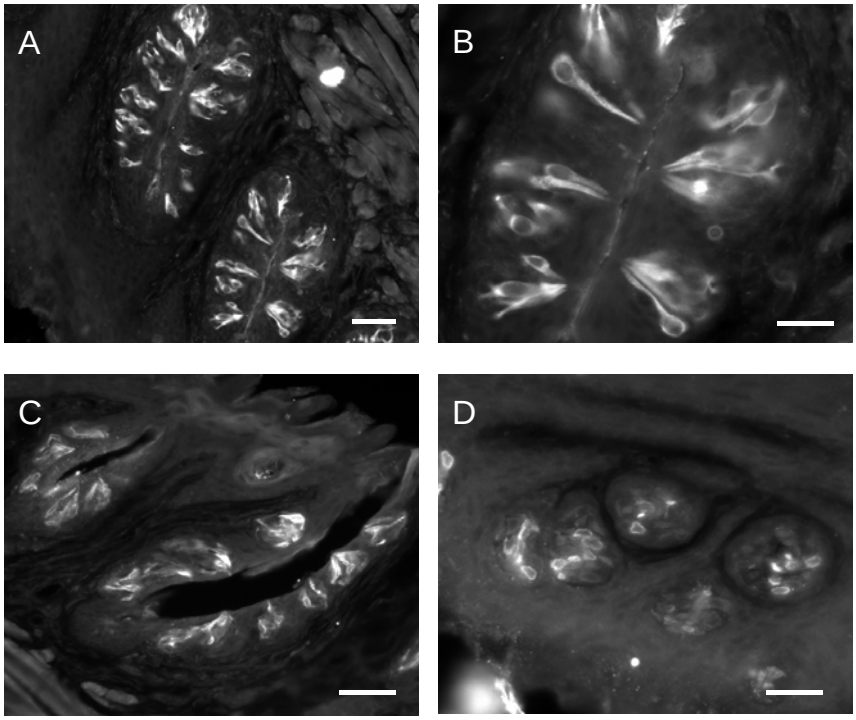

Figure 2.6.1.3 $G\alpha_{gust}$ immunoreactivity in taste cells of mouse foliate and circumvallate papillae. Indirect immunofluorescence using $G\alpha_{gust}$ antibody resulted in specific labelling of taste cells contained in the foliate and circumvallate papillae of the posterior tongue. Taste buds lining the ridges of the folitate papillae were immunopositive for $G\alpha_{gust}$ (A, B). Similarly, the taste buds lining the single, large circumvallate papillae of the mouse tongue (C) contain multiple $G\alpha_{gust}$ expressing cells. Immunopositive cells, identifiable by fluorescent cytoplasm surrounding immunonegative nuclei, are shown in a cross section of circumvallate taste buds (D). In this orientation it is clearly visible that some cells within the taste bud are immunonegative for $G\alpha_{gust}$. Scale bars = 50 µm (B, D) and 100 µm (A, C).

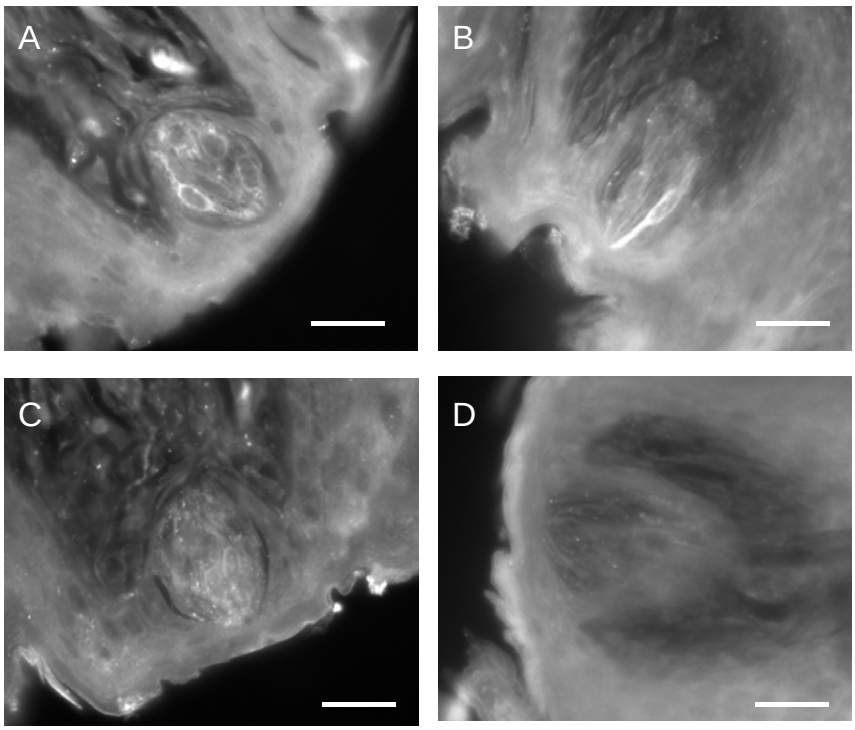

Figure 2.6.1.4 T1R3 immunoreactivity in taste cells of fungiform papillae of the mouse tongue. Immunolabelling with T1R3 polyclonal antibody in sections of the anterior tongue rarely resulted in labelling of cells within taste buds of fungiform papillae (A, B). Although these examples show a single immunopositive cell in a fungiform taste bud these were exceptional examples from all sections assayed for T1R3 immunoreactivity. Most taste buds in fungiform papillae were immunonegative for T1R3 (C, D). A higher background intensity is seen in these images reflecting a longer exposure time confirming the Scale bars = 50 µm.

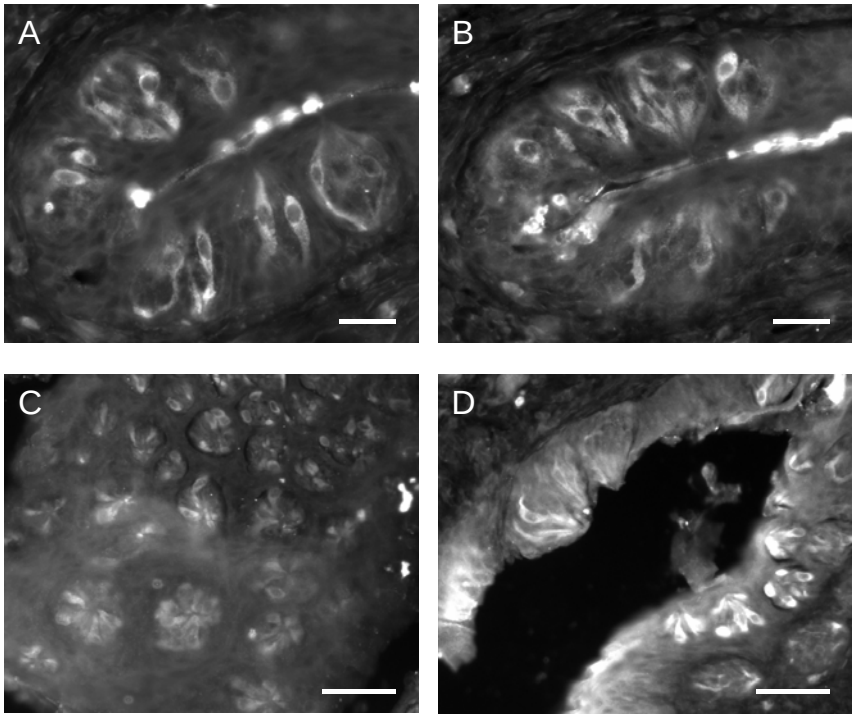

Figure 2.6.1.5 T1R3 immunoreactivity in taste cells of mouse foliate and circumvallate papillae. Indirect immunofluorescence, directed against T1R3 polyclonal antibody, labelled taste cells in taste buds of foliate (A, B) and circumavallate (C, D) papillae in the posterior tongue. Immunoreactivity was homogenous across the cytoplasm as can be seen in the taste cells lining the ridge of the foliate papillae (A, B). A cross-section through circumvallate taste buds shows T1R3 immunoreactivity in a subset of taste cells within each taste bud (C). Circumvallate taste buds lining the groove of the papillae show individual taste cells displaying T1R3 immunoreactivity. Scale bars = 50 µm (A, B) and 100 µm (C, D).

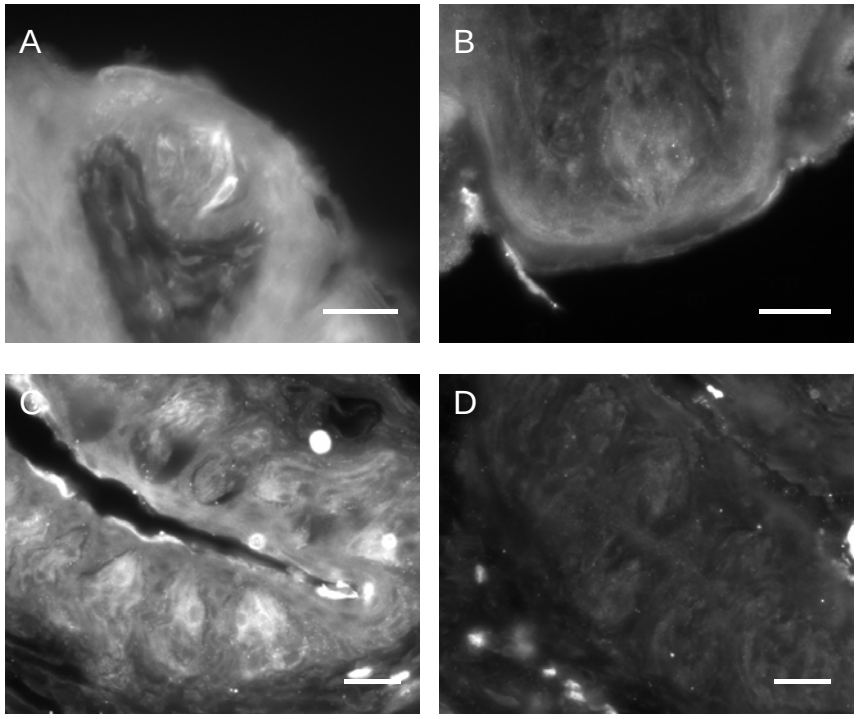

Figure 2.6.1.6 TRPM5 immunoreactivity in taste cells of mouse tongue.
Immunohistochemistry using a polyclonal antibody against TRPM5 in either anterior or posterior tongue did not produce any reliable, specific label of taste cells. A single taste cell in fungiform papillae is shown as immunopositive (A), however this was rare. Most fungiform taste buds are immunonegative (B). In assays of sections of the posterior papillae, some immunoreactivity was evident in taste cells (C). However this labelling was at a lower level than that observed in assays of other taste signal-protein antibodies. Most taste cells in taste buds of the posterior were immunonegative (D). Adjacent serial sections to those containing TRPM5-negative cells had robust, specific label of taste cells when incubated with $G\alpha_{gust}$ or $G\gamma13$ primary antibodies. Scale bars = 50 µm.

$G\alpha_{gust}$ expression in solitary epithelial cells of the mouse small intestine

After confirming immunolabeling and specificity of tabelling in lingual taste cells, the polyclonal $G\alpha_{gust}$ antibody was tested in sections of mouse small intestine. This antibody proved to be a highly effective tool for investigation of expression and localisation of taste-signal protein $G\alpha_{gust}$ in the small intestine.

$G\alpha_{gust}$ immunoreactivitiy was contained within individual cells of the villous epithelium in mouse small intestine (Figure 2.6.1.7). These cells were dispersed throughout the epithelium and surrounded by clearly immunonegative enterocytes. $G\alpha_{gust}$ expressing cells were open cell-type, with their apical tip exposed to the lumen and were often located in the upper villi, near the villous tip. Immunolabeling within individual cells was homogenous across the cytoplasm, although immunolabelling was concentrated at the apex of $G\alpha_{gust}$ expressing cells, often extending above the brush border membrane. $G\alpha_{gust}$ immunopositive cells were rare in most proximal segment of the small intestine but were common in regions beyond the duodenum.

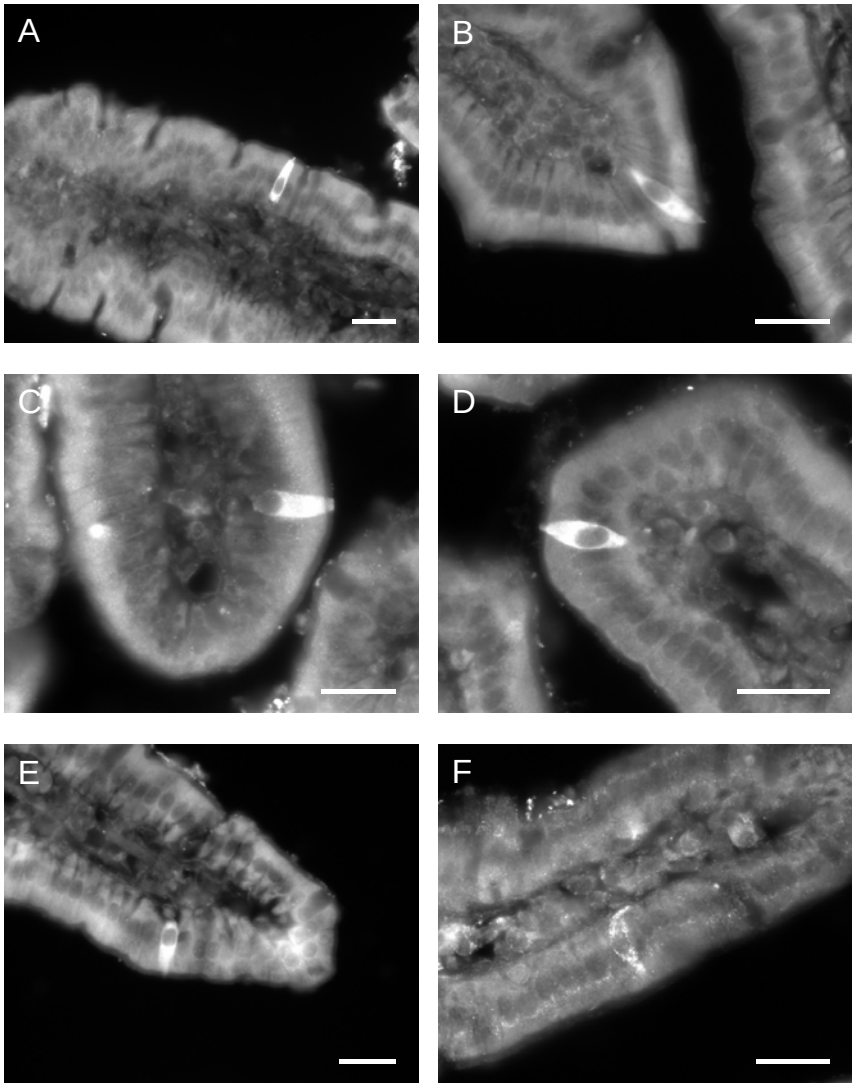

Figure 2.6.1.7 Gα_{gust} immunoreactivity in solitary epithelial cells of mouse small intestine.
Gα_{gust} primary antibody labelled cells in the epithelium of the small intestinal villi (A-F). Immunopositive cells were dispersed throughout the epithelium, clearly distinguishable from surrounding immunonegative enterocytes. A broad apical region and tip was common in these positive cells (C, E). One example of an Gα_{gust} positive cell appears to have a basal projection (F). Gα_{gust} positive cells were most frequently located in the mid to upper villus (A, F) and at the villi tip (B-E). No labelled cells were found in negative control sections where primary antibody was omitted from the assay. N = 6. Scale bars = 50µm.

Gγ13 expression in the epithelium of mouse small intestine

The Gγ13 polyclonal antibody frequently produced a high level of background labelling in small intestinal sections not present in tongue sections. In these sections specific labelling of the primary antibody was difficult to determine, however many intestinal sections contained epithelial cells immunopositive for Gγ13 (Figure 2.6.1.8). These Gγ13 expressing cells closely resembled cells immunopositive for $G\alpha_{gust}$ in both labelling characteristics and distribution. However as both primary antibodies were raised in rabbit that these two proteins were expressed in the same cells was not able to be confirmed by double labelling. All Gγ13 immunopositive cells were open-type and showed labelling throughout the cytoplasm but concentrated at the apical tip. Gγ13 expressing cells were dispersed singularly throughout the epithelium of the villi and were commonly localised in the upper portions of the villus. As with $G\alpha_{gust}$, Gγ13 immunopositive cells were clearly identified from neighbouring enterocytes, although labelling intensity was less than that obtained in $G\alpha_{gust}$ assays.

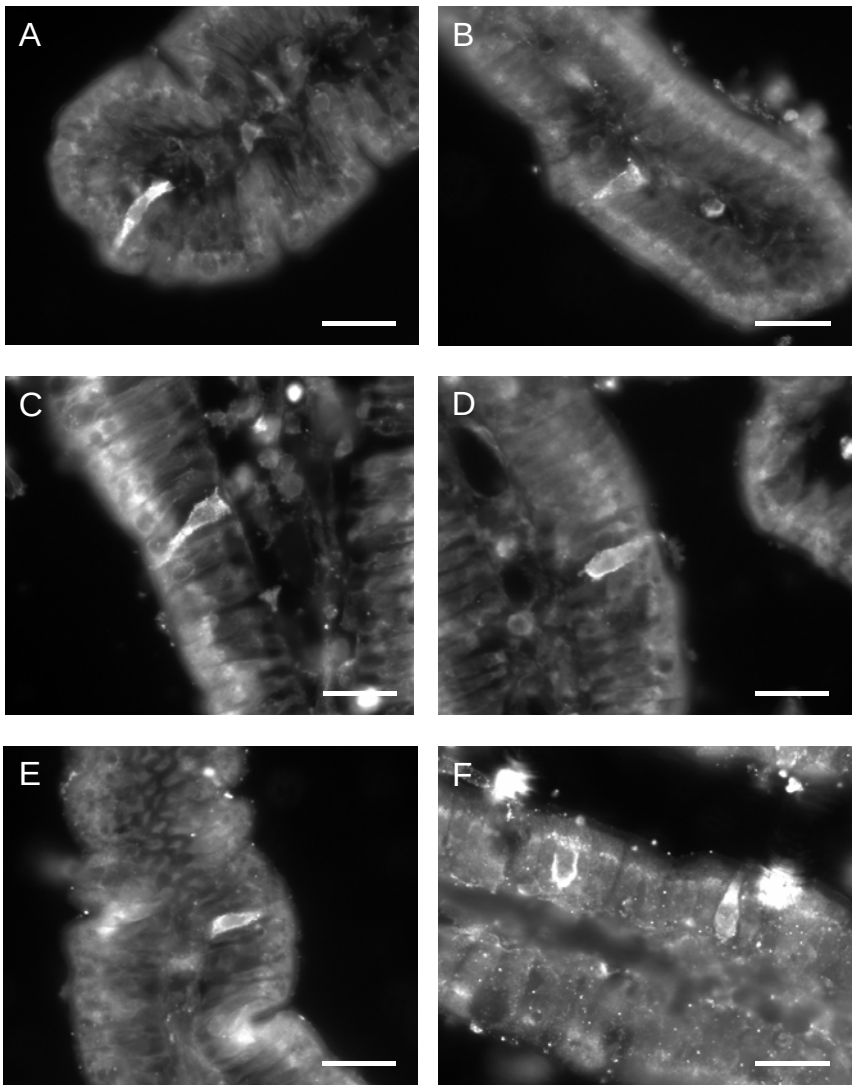

Figure 2.6.1.8 Gγ13 immunoreactivity in solitary epithelial cells of mouse small intestine.
Gγ13 primary antibody labelled epithelial cells of the small intestine (A-F). Immunolabelling was often visibly concentrated at the apical tip of Gγ13-expressing cells (D, F) and these cells were frequently associated with the upper villous epithelium and close to the villus tip (A). Gγ13-labelled cells appeared to most frequent in jejunal sections, with this single villi from the jejunum shown here containing multiple cells (F). No cells were observed in sections where the primary antibody was omitted from the incubation. Scale bars = 50μm.

T1R3 expression in the epithelium of mouse small intestine

Immunolabelling by the T1R3 receptor primary antibody in the small intestine performed similarly to Gγ13 primary antibody, with high background labelling in the majority of tissue sections. Modification of the immunohistochemical protocol did not rectify this problem, making further assessment of T1R3 labelling in intestine difficult. Despite poorer intestinal labelling with the T1R3 antibody overall, positive labelling was seen in three mice (Figure 2.6.1.9). In these sections immunopositive cells were identified within the villous epithelium, and were comparable in labelling and distribution characteristics to $G\alpha_{gust}$ and Gγ13. A number of the T1R3-positive cells, however, did show denser immunolabelling at the apical tip and around the edge of the cell, indicating antibody recognition of a membrane target. Despite problems with labelling quality for T1R3 in the small intestine, fewer T1R3 immunopositive cells were detected compared to $G\alpha_{gust}$ and Gγ13 immunopositive cells within similar gut regions, however same-species antibodies precluded this from being directly tested.

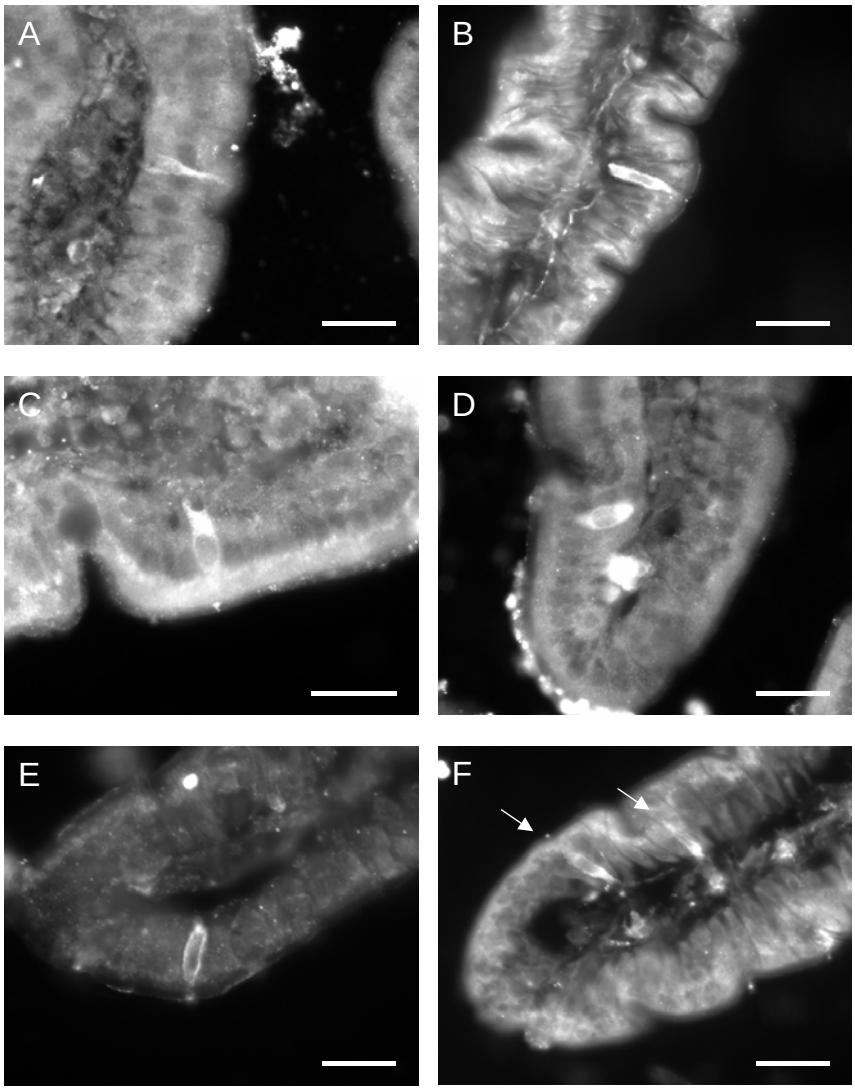

Figure 2.6.1.9 T1R3 immunoreactivity in solitary epithelial cells of the mouse small intestine.
In the small intestine, evaluation of T1R3 labelling was complicated by increased non-specific background levels of fluorescence. Despite this, clear examples of individual epithelial cells expressing T1R3 were identified (A-F). Immunofluorescence was present throughout the cytoplasm with label concentrated in the apical tip of the cell (C, E). Immunolabelling in some cells was concentrated along the membrane of the cell (E) and were located near the villous tips (D-F). Two immunopositive cells are shown in close proximity to a villi tip in the jejunum (F). No cells were labelled in negative controls. N =3.
Scale bars = 50 µm.

TRPM5 expression in the epithelium of mouse small intestine

The failure of the TRPM5 antibody to detect a target in the lingual epithelium indicated it was a suboptimal tool to localise TRPM5 in the small intestine. However TRPM5 immunolabelling was performed in one mouse small intestine for completeness and which resulted in high intensity background labelling. What could be rare immunopositive TRPM5 cells were seen in the epithelium of the small intestine (Figure 2.6.1.10), and labelled in a comparable pattern to the other taste molecules assayed. However no conclusions can be drawn about the results of this assay due to the unconvincing performance of the positive control. An alternative TRPM5 antibody or will have to be manufactured or alternative strategies developed to investigate localisation of TRPM5 protein in the small intestine.

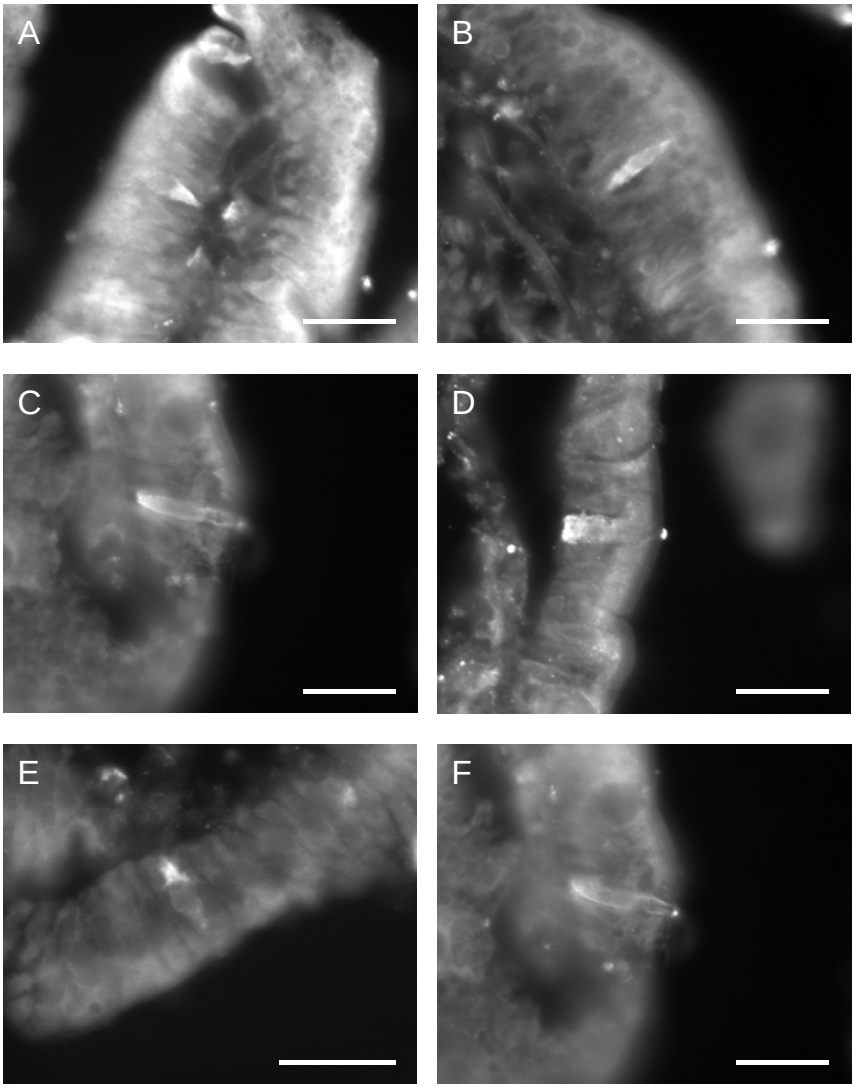

Figure 2.6.1.10 TRPM5 immunoreactivity in the mouse small intestine.
Similar to labelling patterns in positive control tongue sections, no consistent, specific labelling of cells with TRPM5 primary antibody was observed in the small intestine. High levels of background fluorescence, confounded identification of positive cells, however occasional examples of positive labelling in some sections within some assays were observed in singly dispersed cells within the villous epithelium (A-F). Immunofluorescence was cytoplasmic, often concentrated at the apical tip of the cell (C, D, F). These images represent the total of positive cells observed. These immunopositive cells were from jejunal sections. No cells were found in negative control sections however no firm conclusions can be taken from the results of this assay. N = 1. Scale bars = 50 µm.

Immunohistochemical controls in mouse small intestine

Immunohistochemical assays for each antibody were performed in multiple sections across the length of the small intestine from 4-6 mice (with the exception of TRPM5 where the positive control conditions were not met). Positive identification of taste molecules in mouse small intestine was only possible under specific excitation of the flurochrome conjugated to the secondary antibody (Alexa Fluor 546). Positive cells were undetectable under alternate excitation or filters, indicating labelling identified as specific was not due to autofluorescence. Negative controls, where primary antibodies were omitted did not show positive immunolabelling in the villous epithelium, indicating that the positive immunolabelling was due to specific binding of primary antibodies (Figure 2.6.1.11). Gγ13, T1R3 and TRPM5 labelling in animals led to a high level of background fluorescence in the intestinal epithelium (Figure 2.6.1.11 D); in these cases this was most apparent in the crypt regions or villous tips and made positive identification of labelled cells difficult. However, positive labelled cells were identifiable from the majority of background fluorescence, while no cells were present on negative control sections.

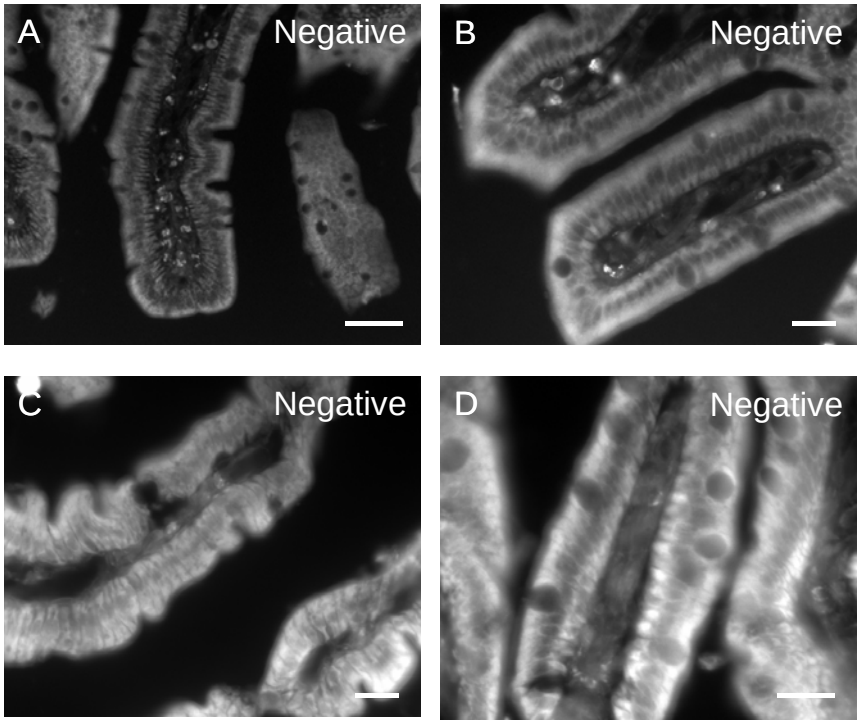

Figure 2.6.1.11 Negative control sections in mouse small intestine.
Negative control sections were included in every assay of taste protein antibodies in the small intestine. In these sections primary antibody was omitted and sections incubated only with the antibody diluent. These sections provided a control for non-specific binding of the secondary antibody to the tissue. No positive cells were identified in these negative control sections (A-D) with the intestinal epithelium completely immunonegative. In some assays and tissues there was a high level of autofluorescence in the epithelium (D). Although this made labelled cells in positive sections hard to image against the high background, cells containing specific label due to primary antibody binding were clearly identifiable from this background fluorescence. Each of these four images were captured at an exposure time equivalent to that which was used to image a positive cell on the same tissue. Scale bars = 50 µm (B-D) and 100 µm (A).

Expression of taste molecule proteins in the myenteric plexus of mouse small intestine

In addition to expression of taste molecules in solitary cells in the villous epithelium, immunolabelling was also observed in the myenteric plexus between the circular and longitudinal muscle layers in cell bodies of myenteric neurons. Labelled myenteric neurons were observed in sections from assays for all four of the taste-signal proteins T1R3, $G\alpha_{gust}$, $G\gamma13$ and TRPM5 (Figure 2.6.1.10). The immunolabelling pattern for each primary antibody reflected that seen in the epithelial cells, with strongest labelling apparent with $G\alpha_{gust}$ followed by $G\gamma13$. T1R3 antibody also labelled myenteric neurons, although at observably lower levels than for the G-protein subunit targets; however this myenteric label was often present in the absence of labelled cells in the epitelium. Results from the single TRPM5 intestine assay showed some example of what could be equivalent labelling, however nothing can be concluded from these findings.

Immunolabelling for taste molecules was primarily associated with myenteric cell bodies between the muscular layers of the intestine, although immunopositive nerve fibres were occasionally observed within the myenteric plexus in transverse sections (Figure 2.6.1.12 F). Immunoassays performed in whole mount tissue also confirmed this myenteric labelling for taste molecules (Figure 2.6.1.13). Further experiments were performed to confirm labelling of taste molecules to neuronal structures (myenteric neurones) by dual-labelling for $G\alpha_{gust}$ or $G\gamma13$ with a monoclonal PGP 9.5 antibody (Ultraclone). In composite images, coexpression of $G\alpha_{gust}$ or $G\gamma13$ was confirmed in PGP9.5 labelled myenteric neurons (Figure 2.6.1.14). The expression of taste proteins in myenteric neurons of the mouse small intestine was not further investigated in these studies.

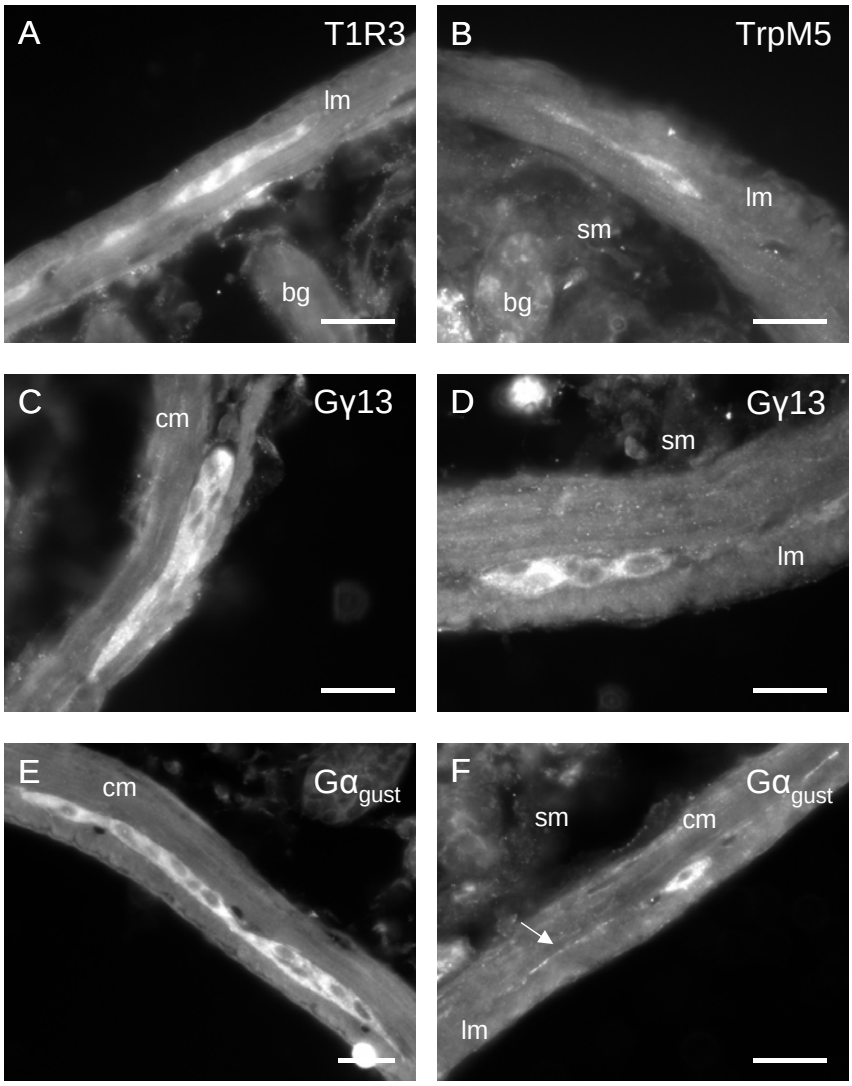

Figure 2.6.1.12 Taste protein immunoreactivity in the myenteric plexus of mouse small intestine. Immunofluorescence for T1R3 (A), Gγ13 (C, D) and $G\alpha_{gust}$ (E, F) (n = 3 animals) was observed in structures resembling neuronal cell bodies in the myenteric plexus between the circular (cm) and longitudinal (lm) muscle layers. A potential example of immunolabel in the myenteric plexus for TRPM5 was also found (n = 1) (B). Labelling in the myenteric plexus appeared strongest and most frequent in assays for the G-protein subunits Gγ13 and $G\alpha_{gust.}$ Immunoreactivity between the muscle layers may indicate an $G\alpha_{gust}$-immunoreactive fibre (F, arrow). sm; submucosa, bg; Brunner's gland. Scale bars = 50 µm.

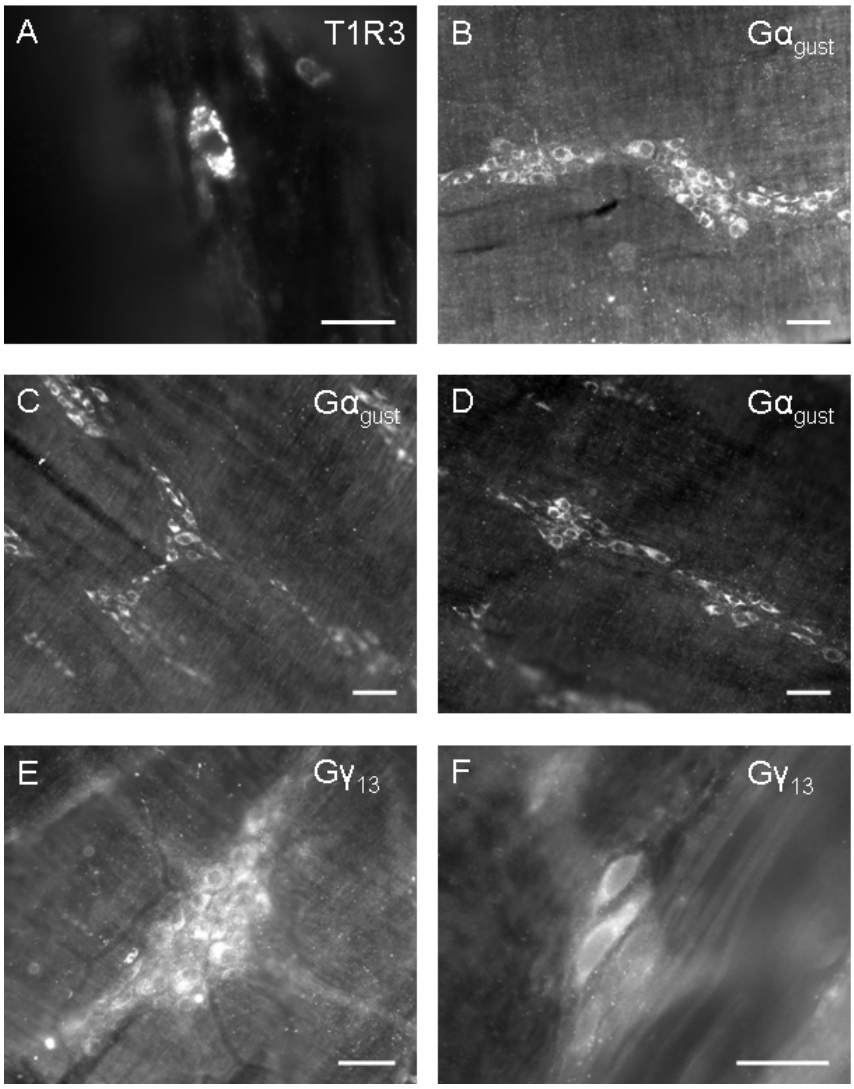

Figure 2.6.1.13 Taste protein immunoreactivity in the myenteric plexus; whole mount muscle layer. Immunoreactivity was observed in what appears to be neuronal cell bodies in ganglia of the myenteric plexus (A-F). T1R3 assays occasionally resulted in immunoreactivity within the cytoplasm of cells in the myenteric plexus (A). $G\alpha_{gust}$ immunopositive cell bodies were visible within myenteric ganglia between the muscle sheets (B-D). Neuronal cell bodies also appeared to be immunoreactive for $G\gamma13$ (E, F). Assays for $G\alpha_{gust}$ resulted in the labelling of the most myenteric cell bodies followed by $G\gamma13$. Scale bodies = 50 µm (A, B, E, F) and 100 µm (C, D).

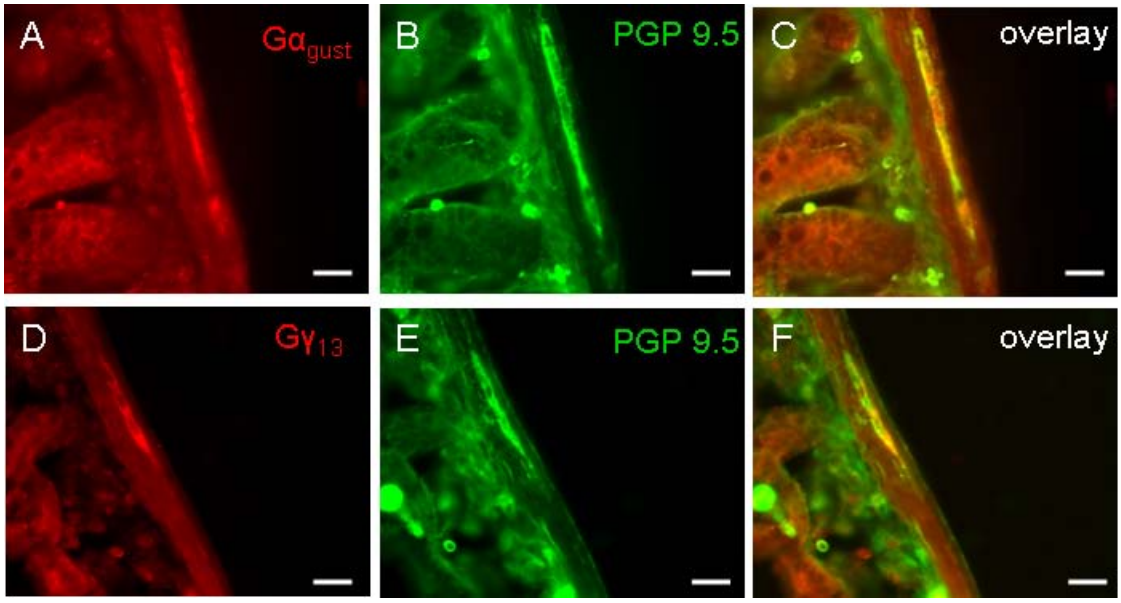

Figure 2.6.1.14 Colocalisation of $G\alpha_{gust}$ and Gγ13 immunoreactivity with neuronal marker PGP9.5 in the myenteric plexus.
Intestinal sections incubated with either $G\alpha_{gust}$ or Gγ13 primary antibody in a double label protocol with a monoclonal antibody for the neuron specific marker PGP 9.5 were visualised with species specific secondary antibodies coupled to alternative fluorophore colours. Individual images taken under specific filters for each fluorophore showed that $G\alpha_{gust}$ (A) and PGP 9.5 (B) and Gγ13 (D) and PGP 9.5 (E) appear to produce immunoreactivity within the same structures in the myenteric plexus. Composite images for $G\alpha_{gust}$ and PGP 9.5 (C) and Gγ13 and PGP 9.5 (F) show yellow fluorescence indicative of colocalisation of the two primary antibodies within the same structures. Scale bars = 100 µm.

2.6.2 RT-PCR

Expression of taste molecules in the mucosa of the mouse small intestine

Specific expression of taste molecules in the mucosa of the mouse small intestine was confirmed using RT-PCR. Amplified PCR products were separated by gel electrophoresis on agarose ethidium bromide gels for UV visualisation and imaging (Figure 2.6.2.1). Resulting images confirm the specificity of the gene specific primers for each target in positive control reactions (Figure 2.6.2.1, A-E, first lane). In all reactions using tongue RNA template, a single intense band corresponding to the predicted amplicon size (as determined by position in relation to the 100 bp interval bands of the molecular weight marker) was observed. RT-PCR reactions with template RNA extracted from the jejunal mucosa showed an identical band (A-E, third lane) indicating amplification of the gene specific products. No bands were observed in NT controls reactions confirming that products were amplified specifically from template and that no contamination of reactions occurred. In –RT control reactions using primer assays for T1R2, $G\alpha_{gust}$ and TRPM5 no bands were visible, confirming amplification occurred from specifically expressed transcripts and not contaminating genomic DNA. In the case of T1R3, two alternative primers were compared in separate reactions (B, C); both produced single bands corresponding to the specific amplicon size. Despite primers for T1R3 being designed to span an intron to avoid gDNA coamplification, -RT controls in some samples showed a faint band the same size as the predicted amplicon size. As no reverse transcription took place in these reactions and corresponding NT controls produced no product, it appears that contaminating gDNA in the sample served as template in these reactions. Although bands were observed in some –RT reactions they were much fainter in appearance than those produced from PCR reactions where RNA template underwent reverse transcription. For example, the mucosal sample produced an intense single band, whereas the band in the –RT control at the same size was barely visible (Figure 2.4.2.1B). This suggests that even

though product amplification occured from gDNA present in the sample, this constitute only a minor portion of the accumulated PCR product and most of the signal was specifically amplified from mRNA. In all PCR reactions for T1R3 the substantially higher intensity of bands in RT-PCR reactions than –RT controls confirms that T1R3 is expressed specifically in jejunal mucosa.

RNA extracted from kidney tissue served as a negative control for expression of taste molecules. Reactions using primers for T1R2 (A) and $G\alpha_{gust}$ (D) showed no bands indicating no amplification from kidney RNA template. This demonstrates that the taste receptor T1R2 and $G\alpha_{gust}$ are not expressed in the kidney and confirms that the kidney is a suitable negative control tissue for expression of these transcripts. A band of the predicted amplicon size for TRPM5 (E) was detected at marginal levels after gel electrophoresis of PCR product from kidney template reactions. This suggests TRPM5 may be expressed in the kidney, although at levels much lower than in tongue or intestine. In a similar manner, a specific band for T1R3 (B, C) was found in PCR product from reactions using kidney template. As the T1R3 primer assays appear to amplify gDNA if present, a –RT control was run using kidney template. A faint band of the correct size was present in the –RT controls, but as was the case with mucosal samples, the intensity of this band was an order of magnitude less than that produced by RT-PCR reactions. The difference in the intensities of these bands reflect product specifically amplified from kidney mRNA and suggest that T1R3 may indeed be expressed in the kidney.

All RNA samples of each tissue type were run in PCR reactions with primers for β-actin to serve as an endogenous control for the RT-PCR method. A single band corresponding to the amplicon size of β-actin (A-E) was produced from mucosal template in all reactions, validating the sample RNA and gene-specific expression data obtained by RT-PCR.

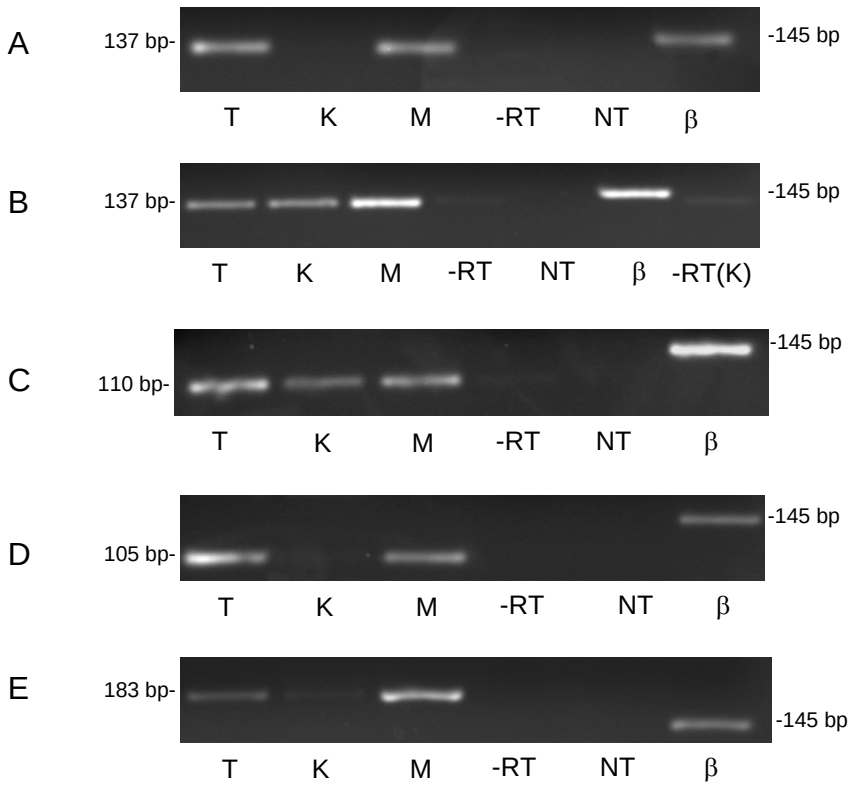

Figure 2.6.2.1 Expression of taste molecules in the mucosa of the mouse small intestine detected by RT-PCR and gel electrophoresis.
A single band corresponding to the predicted size of T1R2 (A), T1R3 (B, C), $G\alpha_{gust}$ (D) and TRPM5 (E) amplicons was confirmed in the RNA from circumvallate epithelium of the tongue (T). An identical product was also amplified from RNA template from the mucosa (M). PCR amplification of kidney RNA samples (K) did not show a positive signal for T1R2 or $G\alpha_{gust}$ whereas a faint band resembling the correct product was visible in TRPM5 reactions while T1R3 appeared to be specifically expressed in this tissue. In endogenous control reactions for the RT-PCR a single specific band for β-actin (β), was observed in the mucosal samples. No reverse transcription (-RT) and no template (NT) control reactions did not show any amplified product on the gel.

Regional expression data of taste molecules in mouse small gastrointestinal tissue

Quantification of taste molecule transcript levels in the mouse small intestinal mucosa was performed by analysis of SYBR green fluorescence data acquired during real time RT-PCR reactions. Regional expression levels of each taste molecule transcript along the small intestine are presented in Figure 2.6.2.2. T1R2 transcript levels in the small intestine showed region-specific expression patterns with levels in the jejunum significantly higher than in the duodenum ($p < 0.05$) or the ileum ($p < 0.0001$, A) with jejunal transcript levels 2.1-fold higher than the duodenum and 8.8-fold higher than the ileum. T1R2 transcript levels were lowest in the distal small intestine although there was no significant difference in expression levels between the duodenum and ileum. Although mean expression of T1R3 transcripts (B) was marginally higher expression in the duodenum, T1R3 transcripts were not expressed at significantly different levels between the three regions of the small intestine. $G\alpha_{gust}$ transcript expression (C) was highest in the ileum where levels were 28.8-fold higher than in the duodenum ($p < 0.001$) and 5.7-fold higher than in the jejunum ($p < 0.001$). Although levels of $G\alpha_{gust}$ transcripts increased with distance from the pylorus with peak expression in the ileum, this did not attain statistical significance in comparisons between expression in the duodenum and jejunum. TRPM5 (D) transcripts, in contrast, showed no regional expression pattern with transcript levels relatively constant between mucosal samples from all three regions.

Levels of taste molecule transcripts were also quantified in the distal esophagus and the gastric fundus, body and antral mucosa, as shown in Figure 2.6.2.3i. All samples from the three gastric regions were averaged and graphed with averaged values from proximal intestine samples (duodenum and jejunum) to compare relative expression levels between the stomach and the intestine (Figure 2.6.2.3 ii).

Transcripts for T1R2 were not detected in real time RT-PCR reactions with esophageal samples. Similarly no amplification of target occurred in mucosa samples from the gastric fundus or body. However, a late

amplification curve was detected in around half the reactions from the gastric antrum, while other reactions were negative. The product generated in these reactions was specific for T1R2 amplification based on melt curve analyses and gel electrophoresis. This indicated that T1R2 was present at low levels in the gastric antrum, which in many samples may have been below the detection threshold of the PCR reaction. These data show that T1R2 transcript is preferentially expressed in the small intestine in the mouse upper gastrointestinal tract with negligible levels present in the mucosa of the gastric antrum.

T1R3 transcripts were specifically expressed in esophagus and stomach samples in real time PCR assays. No amplification occurred in –RT controls performed for each regional sample, confirming that mRNA from each region served as template for the amplification of T1R3 transcript. Comparison of gastric levels of T1R3 transcripts with that in the small intestine revealed that intestinal expression was 3.9-fold higher than that in stomach ($p < 0.0001$), indicating regional differences in expression in the mouse upper gastrointestinal tract.

$G\alpha_{gust}$ mRNA was expressed at low levels in the esophagus and in mucosa of the gastric fundus and body, with no significant difference in expression between these regions. The mucosa of the gastric antrum, however, expressed high levels of $G\alpha_{gust}$ transcript - 2.5-fold higher than in ileum, the region of highest expression within the small intestine. Comparison of $G\alpha_{gust}$ transcripts levels between stomach and proximal intestine revealed transcripts were 10.5 times more abundant in the gastric mucosa ($p < 0.05$). Transcripts for $G\alpha_{gust}$ in the upper gastrointestinal tract in mouse therefore display distinct regional specificity with peak expression evident within the gastric antrum.

TRPM5 transcripts were not detected in the esophagus and low levels only were expressed in the gastric fundus and body. Like $G\alpha_{gust}$, levels of transcript for TRPM5 were highest in the gastric antrum where expression was 5.1-fold higher than in the gastric body ($p < 0.001$). Despite this higher expression in the

antrum sample, there was no statistically relevant difference between TRPM5 expression in gastric and small intestinal regions.

In addition to determining regional expression of taste molecule transcripts, relative levels were also compared within the tongue and each region of the gastrointestinal tract (Figure 2.4.2.4). Analysis of real time RT-PCR data from the circumvallate epithelium revealed that $G\alpha_{gust}$ transcript was expressed at significantly higher levels than other taste molecule transcripts - 4.4 times higher than T1R3 ($p < 0.001$). In contrast there were no significant differences in expression of T1R2, T1R3 and TRPM5 in tongue. TRPM5 transcript levels in the gastrointestinal tract, however, were markedly different – expression of TRPM5 and $G\alpha_{gust}$ transcript was comparable in the gastric antrum and significantly higher here than for T1R2 and T1R3 ($p < 0.001$). However TRPM5 was the most abundant transcript in small intestinal regions ($p < 0.05$), with TRPM5 transcripts present in the jejunum in abundance (5:1) compared to T1R3 transcripts. These results highlight important differences in expression of taste molecule transcripts between the tongue and gastrointestinal tract.

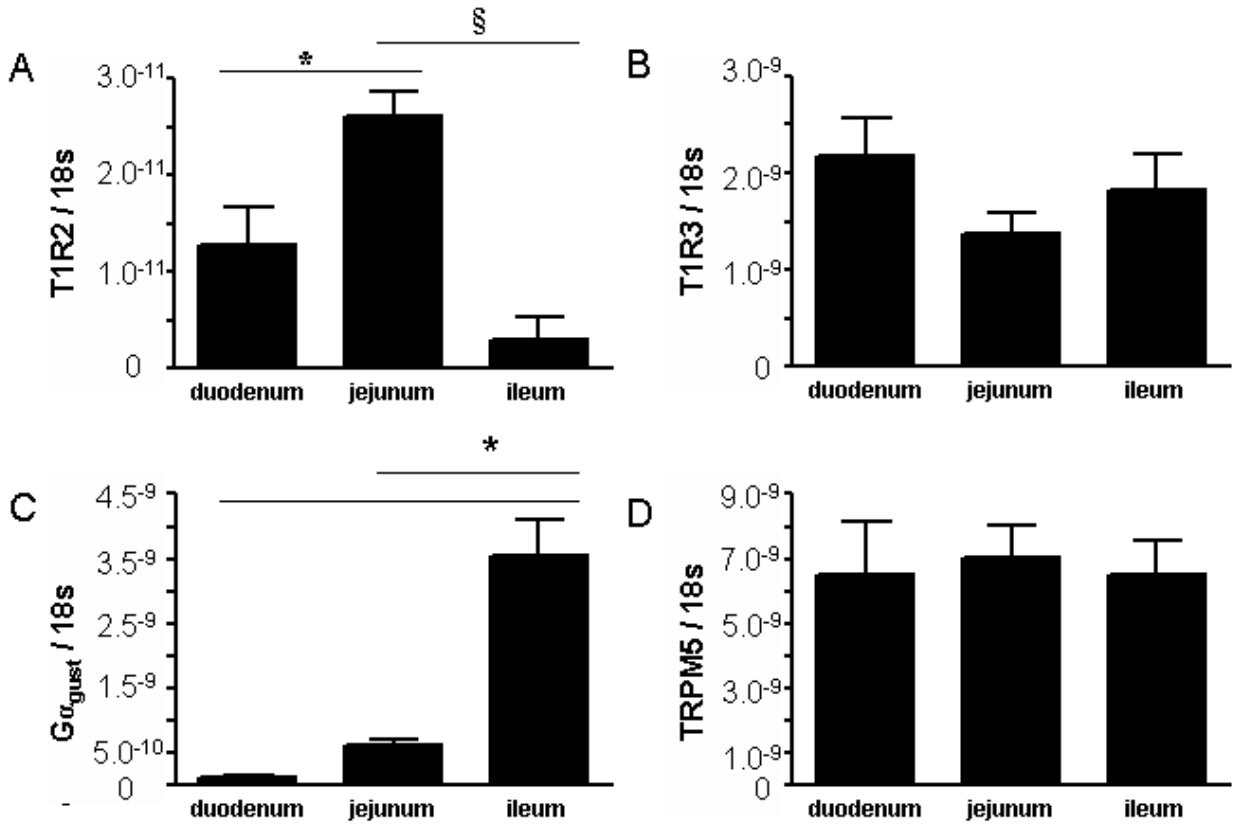

Figure 2.6.2.2 Regional expression levels of taste transcripts in mouse small intestine.
Real time RT-PCR expression data of each taste transcript level relative to 18s rRNA are compared in RNA samples from the mucosa duodenum, jejunum and ileum. A: T1R2 transcript expression levels were significantly higher in the jejunum compared to the duodenum (* $p < 0.05$) and ileum (§ $p < 0.0001$). Jejunal T1R2 expression levels were on average 2.1-fold higher than those in the duodenum and 8.8-fold higher than levels in the ileum. B: T1R3 transcript expression levels were not significantly different between the three regions of the small intestine. C: $G\alpha_{gust}$ transcript levels were significantly higher in the ileum compared the duodenum and jejunum (* $p < 0.001$). Levels of transcript were on average 5.7-fold higher in ileum mucosal samples than those obtained from the jejunum. D: TRPM5 transcript expression was not significantly different between the three regions of the small intestine. Mean ±SEM, N = 3.

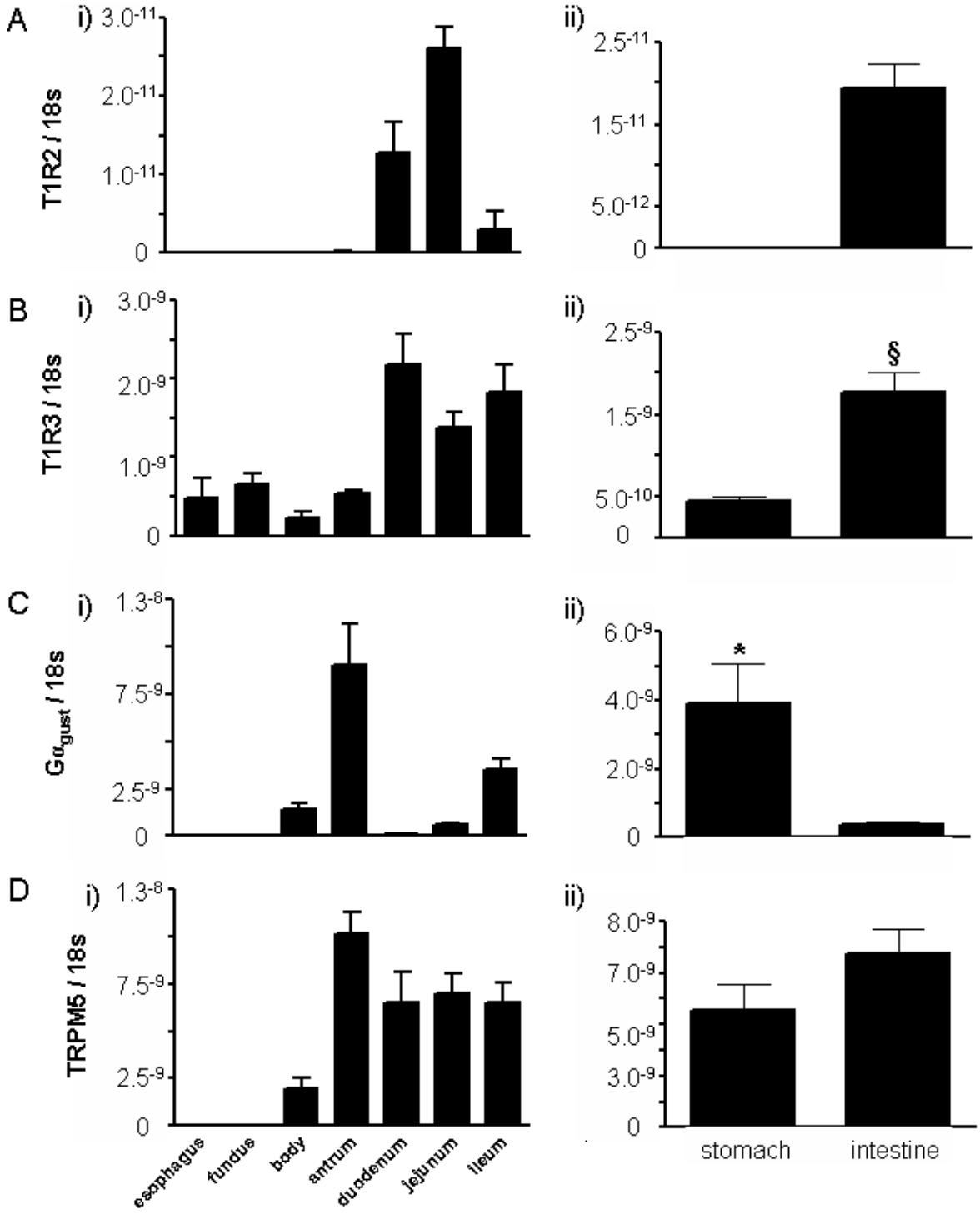

Figure 2.6.2.3 Regional expression levels of taste transcripts along the mouse upper gastrointestinal tract.

Regional expression profiles of T1R2 (A), T1R3 (B), $G\alpha_{gust}$ (C) and TRPM5 (D) transcripts along the upper gastrointestinal tract (i). Transcript levels were averaged across gastric and proximal intestine (duodenum and jejunum) samples to compare expression between the stomach and intestine (ii). The small intestine is the preferential site of T1R2) and T1R3 transcript expression in the upper GI tract (§ $p < 0.0001$). $G\alpha_{gust}$ transcript expression was significantly highest in the gastric antrum (* $p < 0.05$) while TRPM5 transcript levels were not significantly different between gastric and proximal intestinal samples. Mean ± SEM, N = 3.

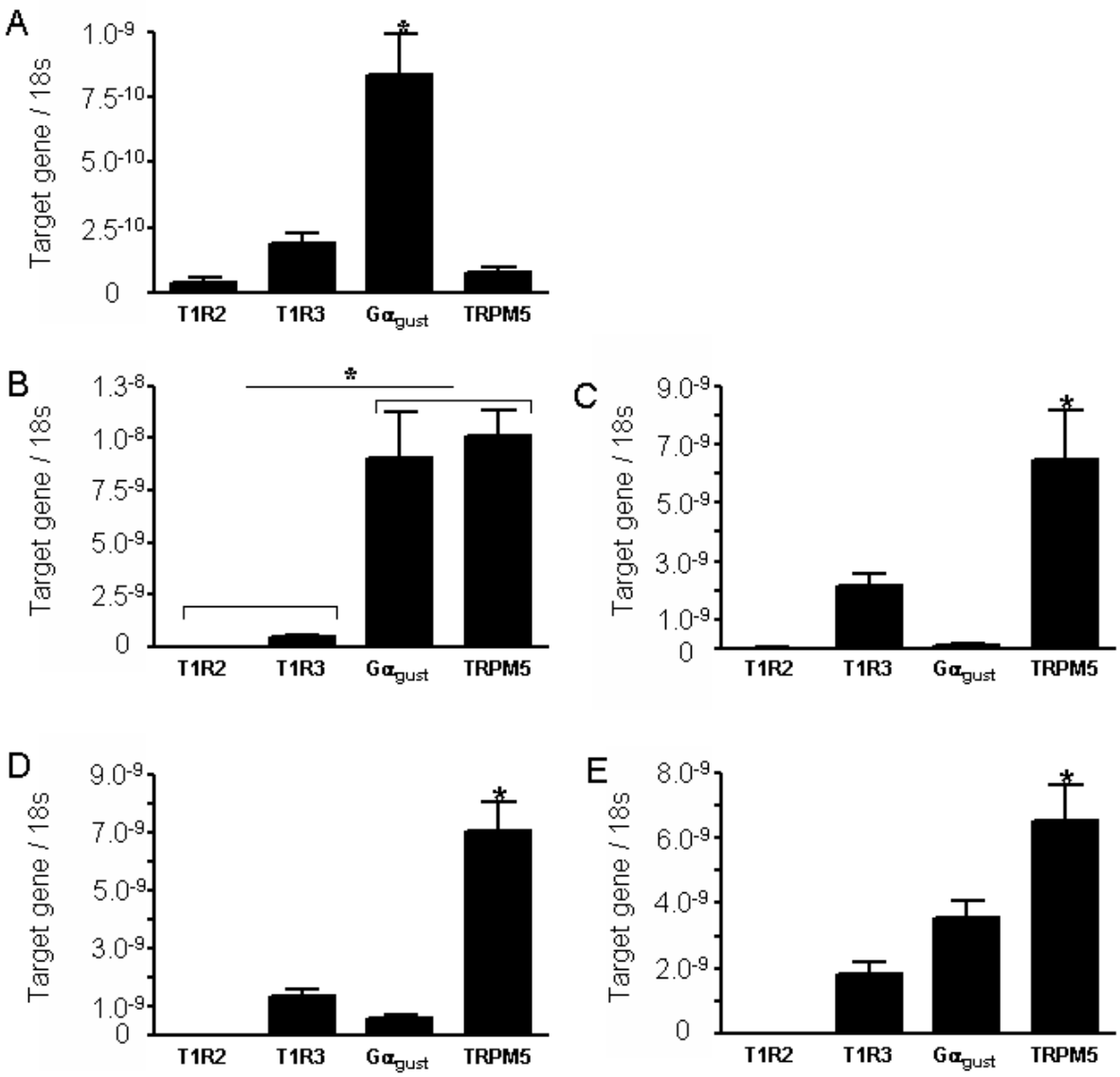

Figure 2.6.2.4 Relative abundance of taste molecules in tongue, antrum and small intestine.
The relative expression of the key four taste molecules were assessed in tongue positive control tissue (A). In the taste-bud containing circumvallate epithelium $G\alpha_{gust}$ was expressed at significantly higher levels than all other taste transcripts (* $p < 0.001$). In the gastrointestinal tract $G\alpha_{gust}$ was preferentially expressed in the antrum of the stomach. In the antrum (B) $G\alpha_{gust}$ and TRPM5 are present at comparable levels but significantly higher than either T1R2 or T1R3 (* $p < 0.001$). However in the small intestine the most abundant taste transcript was TRPM5. In the duodenum (C), jejunum (D) and ileum (E) TRPM5 is expressed in significantly higher levels than all other taste transcripts (* $p < 0.05$). Mean ± SEM, N = 3.

Optimisation and verification of SYBR Green real-time RT-PCR data

For real time RT-PCR data to be meaningful proper optimisation and validation of data and analysis methods must be undertaken. The specificity and quality of real time PCR reactions in these studies was confirmed by a number of control observations. Firstly, real time PCR amplification curves, which show the acquisition of fluorescence with cycle number for each target and reference reaction, all displayed characteristic sigmoidal shape (Figure 2.6.3.1). Low background fluorescence was observed in early cycles before significant accumulation of product. A steep increase in the fluorescence curve indicated linear amplification efficiency during the active phase of the reaction with a high plateau reached as reaction components were depleted. The fluorescence threshold of 0.05 corresponded to the early exponential phase in all reactions. Reference and target reactions reached threshold in order of predicted abundance with 18s the first curve to register, followed by β-actin followed by target taste-signal molecules. No amplification curves were generated in NT controls.

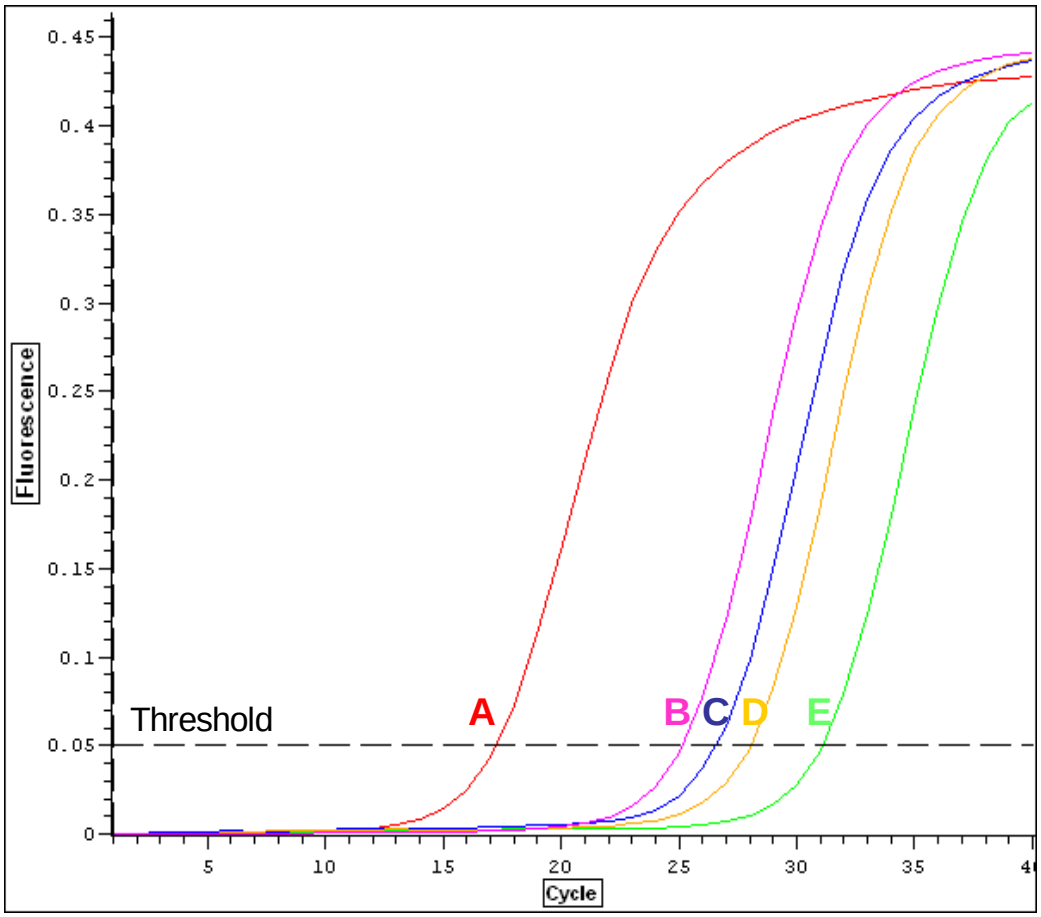

Figure 2.6.2.5 SYBR green fluorescence PCR amplification curves generated in Opticon Monitor software.

Fluorescence acquisition at the end of each PCR cycle plotted against cycle number produces an amplification curve allowing visual representation of the accumulation of PCR product in real time. The validity of the kinetic RT-PCR can be seen in the characteristic shape of the curve recording low background fluorescence, a steep increase in fluorescence indicating linear amplification efficiency and a high level plateau. Five amplification curves from separate real time reactions are shown for β-actin (A), TRPM5 (B), T1R3 (C), $G\alpha_{gust}$ (D) and T1R2 (E) primers with mucosal RNA template. The threshold line is set at 0.05 corresponding to the early exponential phase of the reaction where amount of amplified target is directly proportional to the input amount of target. The corresponding cycle number at which each curve crosses the threshold, the C_T value, is used in subsequent analysis. The lower the C_T value the higher the initial amount of target in the sample. In this figure C_T is first reached by sample A and several cycles later followed by B than C, D and E. This pattern is indicative of the expression levels of these transcripts where β-actin>>TRPM5>T1R3> $G\alpha_{gust}$ >T1R2.

Secondly, the intra-assay variability assessed by coefficient of variance (CV) of the C_T values obtained from reaction replicates was low, indicating high test precision. Table 2.6.2 displays the CV of reactions for each transcript in each sample - in most cases there is less than 1% variation between test replicates. Additionally variability due to the biological sample appeared to be low. Table 2.6.2 also shows inter-sample variability by comparing the averaged C_T values from each biological sample. In this case there was less than 3% variation in C_T values for each transcript, suggesting the results obtained would be consistent across a larger sample group.

Table 2.6.2 Intra-assay and inter-sample variability in jejunum C_T values for real time RT-PCR data analysis.

Primer	sample	Intra-assay		Inter-sample	
		C_T (mean)	CV (%)	C_T (mean)	CV (%)
	1	30.16	0.73		
T1R2	2	30.89	0.6	30.79	1.9
	3	31.32	0.65		
	1	26.97	0.06		
T1R3	2	27.09	0.18	26.87	1.1
	3	26.55	0.27		
	1	27.55	2.7		
$G\alpha_{gust}$	2	27.35	0.17	27.64	1.3
	3	28.03	0.18		
	1	24.78	0.4		
Trpm5	2	24.78	0.53	25.17	2.7
	3	25.94	3.6		

Intra-assay; coefficient of variance (CV) calculated from reaction replicates of each sample indicating test precision, Inter-sample; CV calculated between the mean values of each sample indicating biological variation.

Thirdly, melt curves of fluorescence versus temperature (Figure 2.6.3.2.i) for each reaction product displayed a gradual decrease in fluorescence prior to a steep decline, indicating that upon reaching T_m the rapid loss in fluorescence was due to separation of double stranded product. Melt curve analyses (Figure 2.4.3.2.ii) of the first negative derivative of the fluorescence (-dF/dT) for each reaction displayed a single peak indicating a single specific product had been amplified and that no primer dimers formed during the reactions. Any reactions in which the melt curves deviated from the specific peak for each product (n = 2 tubes total) were discarded from subsequent analyses. Selected reactions were additionally processed by gel electrophoresis to further confirm the presence of a single band of the predicted product size.

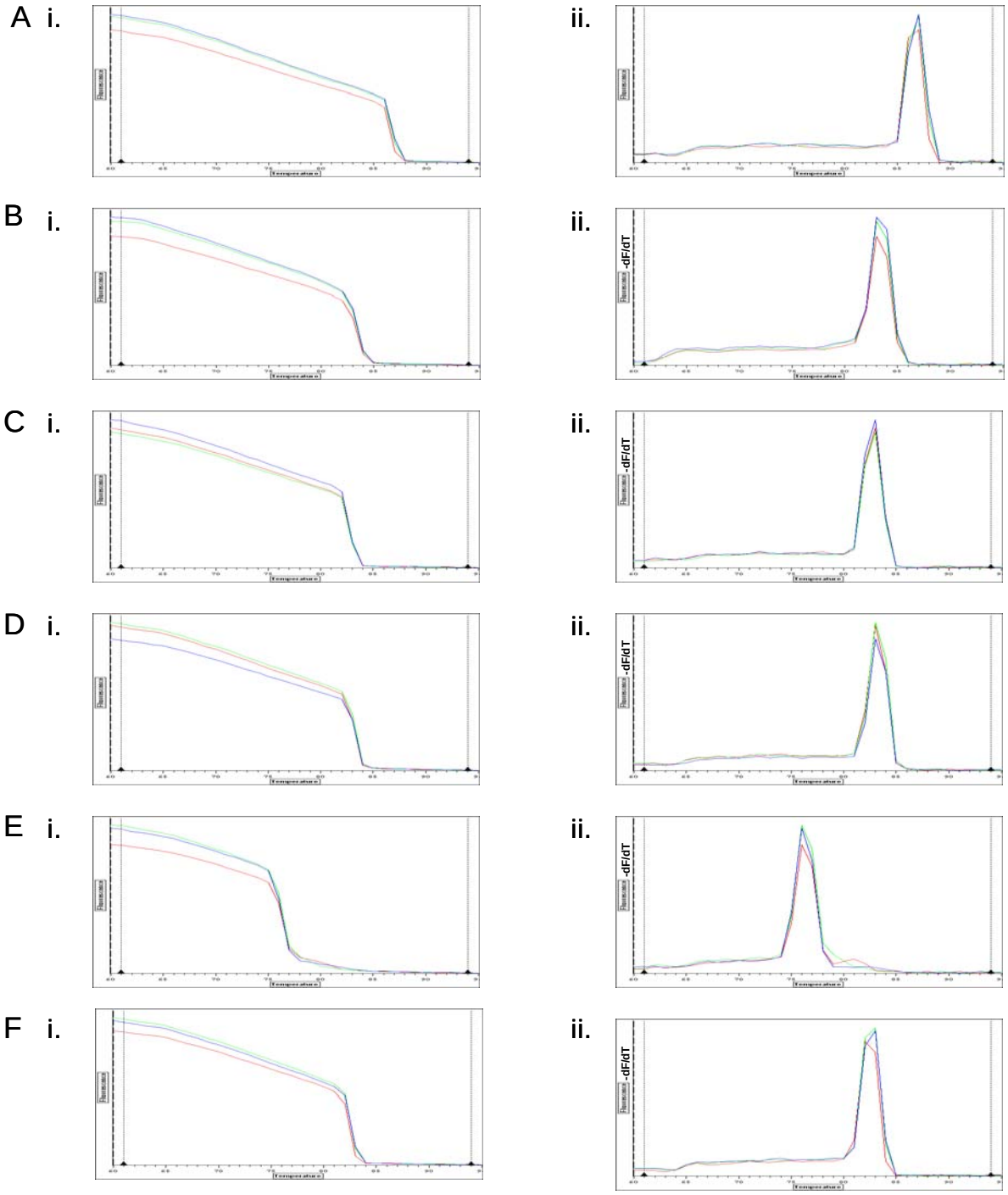

Figure 2.6.2.6 Melting curve analyses for product characterisation.
At completion of the real time cycler programme a melting curve was generated. The melting curves for samples amplifiying β-actin (A), 18s rRNA (B), T1R2 (C), T1R3 (D), $G\alpha_{gust}$ (E) and TRPM5 (F) are shown (i). Fluorescence plotted against temperature shows a gradual decrease in signal due to temperature-dependent quench and a sharp decrease when the melting temperature (T_m) of the product is reached. Analyses are performed by plotting the first negative derivative (-dF/dT) of the melting curve (ii). The resulting single peaks for each reaction confirm a single T_m and therefore amplification of a single product. This validates that no non-specific products were coamplified and confirms an absence of primer dimers.

For each primer assay for target and reference genes a real time PCR standard curve was performed using template RNA in a five log dilution series (100, 50, 25, 12.5 and 6.25 ng RNA). The C_T values obtained were plotted against the log-transformed template concentrations to produce a standard curve for each primer reaction. The result should be a linear graph with a high correlation coefficient. Standard curves for all primers used are presented in Figure 2.6.2.3 with all showing a linear relationship. The slope equation and r^2 (coefficient of determination) are displayed on each graph and in all cases the correlation coefficient (r) approached a value of 1, satisfying the requirement of an $r \geq 0.99$ for use in gene quantification analyses and r^2 values ≥ 0.95.

Finally, in addition to the quantification method, the internal reference gene used in calculations was validated for stability across tissue samples. This was achieved by use of the $2^{-\triangle C_T}$ equation (196) in which levels of β-actin and 18s rRNA were compared in all gastrointestinal regions relative to an internal reference (tongue expression levels, ie $\Delta C_T = C_{T\ \text{sample tissue}} - C_{T\ \text{tongue tissue}}$). Figure 2.6.2.4 shows the relative expression profiles for each internal control. Samples from all regions of the small intestine contained significantly higher levels of β-actin compared to esophageal and gastric samples (A). Furthermore, relative β-actin levels were significantly higher in jejunum than the ileum, consequently this gene was not used as the reference for comparing between tissue regions. In contrast, transcript levels for 18s RNA (B) were relatively stable between all tissues, with no significant difference in expression. In this manner, 18s RNA was validated as an appropriate reference when comparing taste molecule transcript expression levels between these different tissue types.

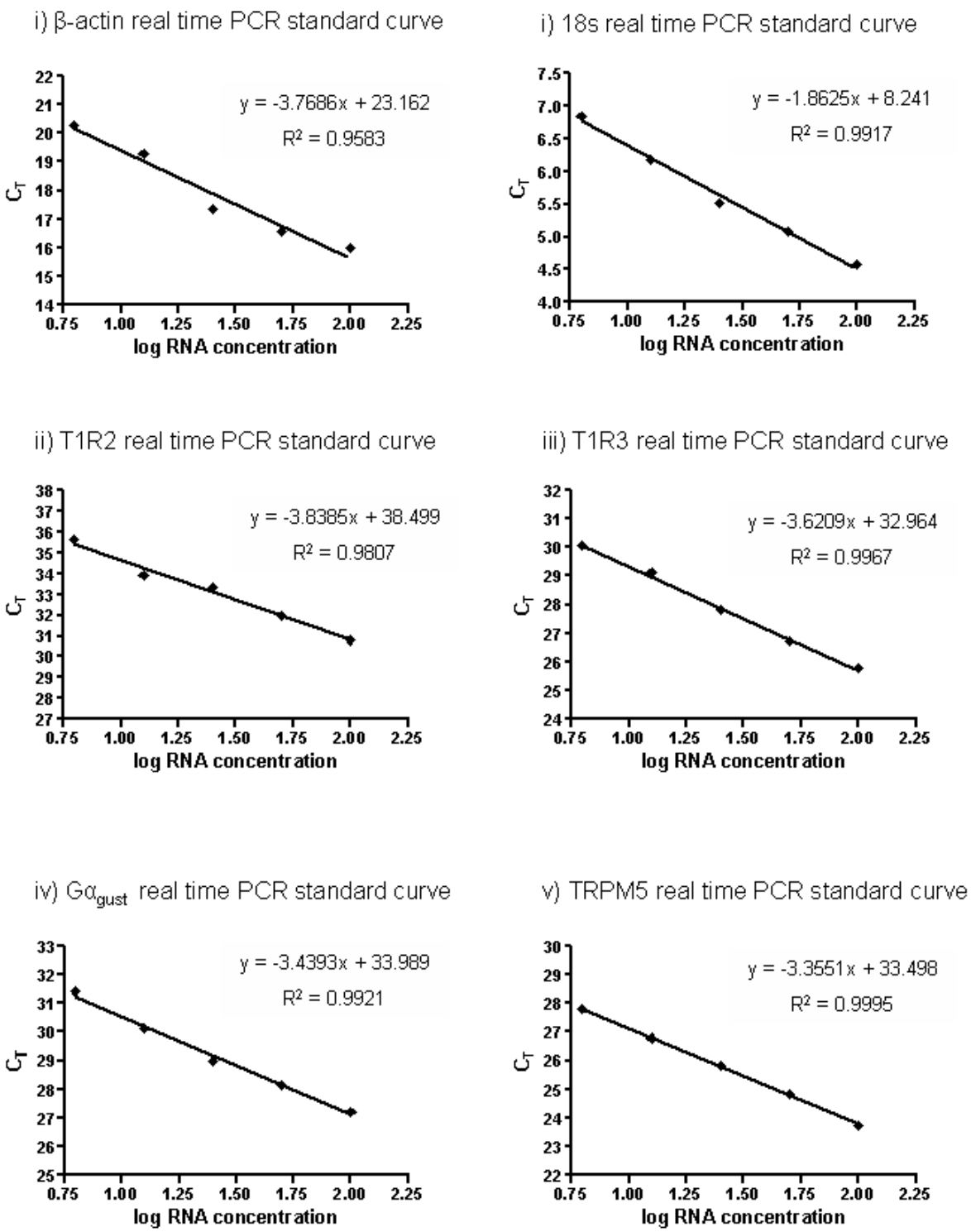

Figure 2.6.2.7 Real time PCR standard curves.
C_T values obtained from a series of five RNA template dilutions (100, 50, 25, 12.5 and 6.25ng) were used to create real time PCR standard curves for each target and reference reaction. Each of the resulting linear graphs show a high correlation coefficient ($r \geq 0.97$) and coefficient of determination ($r^2 > 0.95$) validating the assays for gene quantification. The slopes of the standard curves can be used to calculate amplication efficiency with a slope of -3.3 corresponding to an efficiency of 1 or 100%.

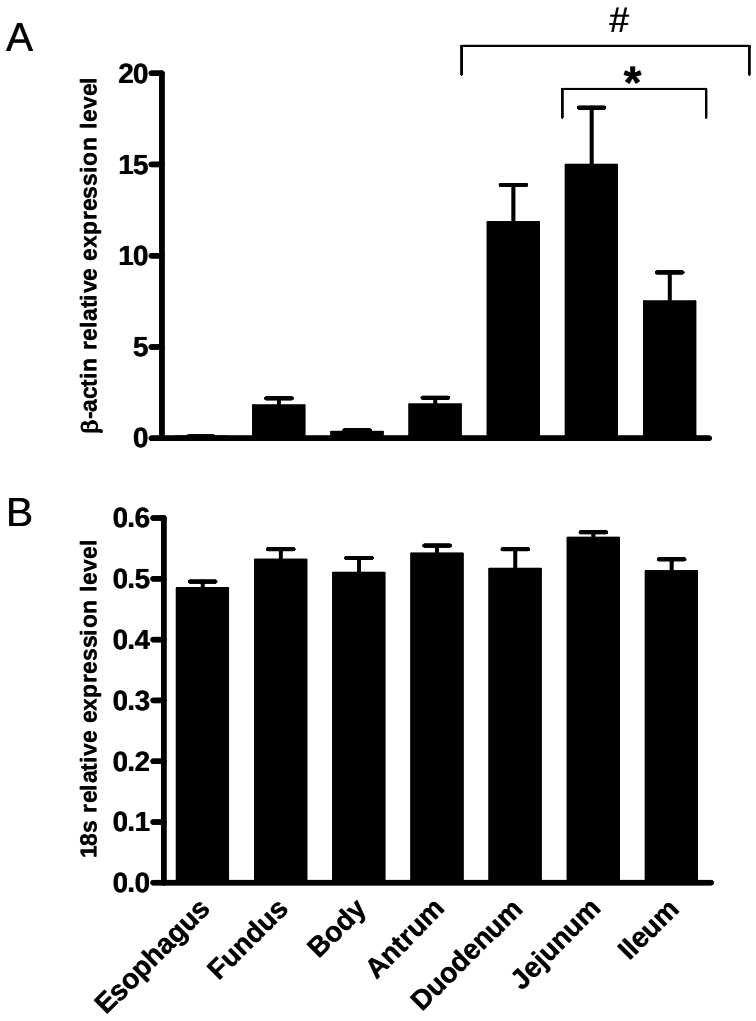

Figure 2.6.2.8 Assessment of appropriateness of reference genes for comparisons between different gastrointestinal tissues.

For a transcript to serve as an appropriate reference for normalisation of real time data it must be stable in its expression levels across experimental samples. Levels of two internal references, β-actin and 18s, were assessed for their expression levels in all gastrointestinal tissue types. This was achieved by using the $2^{-\triangle\triangle C_T}$ method to calculate the relative amounts of each transcript in each tissue type compared to a baseline tissue. Results show that β-actin (A) levels vary significantly between gastrointestinal tissues. β-actin transcripts were significantly higher in all small intestinal regions than in esophageal and gastric samples (# $p < 0.05$). Furthermore within the small intestine, expression is significantly less than in the jejunum (* $p < 0.05$). On the other hand 18s (B) showed no significant difference in levels between any tissue type. This deemed 18s to be a suitable reference to compare taste transcript levels between gastrointestinal regions and was used as the normaliser in all across-tissue comparisons.

2.7 Discussion

The studies in this chapter confirm the specific expression of taste molecules in the mucosa of the mouse small intestine at both transcript and protein level. Although the intestinal mucosa is able to detect and respond to luminal nutrients, the initial molecular recognition events have remained elusive. The identification of key molecules involved in lingual taste transduction within the gastrointestinal mucosa provides the first molecular model for intestinal chemosensation. The presence of sweet taste receptors T1R2 and T1R3 as well as transduction molecules $G\alpha_{gust}$, $G\gamma13$ and TRPM5 strongly indicate that a taste pathway similar to that in the tongue exists in individual epithelial cells in the gut. These taste signal molecules are therefore likely to represent a key trigger for nutrient-induced feedback control of gastrointestinal reflex functions such as gastric emptying and regulation of food intake.

The specific expression of T1R2, T1R3, $G\alpha_{gust}$ and TRPM5 was confirmed in intestinal mucosal samples by amplification of a single RT-PCR product of the predicted size, which was identical to amplified product from lingual positive control samples. Expression of T1R2, $G\alpha_{gust}$ and TRPM5 transcripts were detected in lingual and intestinal samples, supporting a specific chemosensory role, but were absent from renal negative control samples. Expression of T1R3, however, occurred without co-expression of other taste transduction elements in kidney samples and does not directly support the presence of a 'taste' pathway in the kidney.

Previous studies have identified the expression of $G\alpha_{gust}$ transcript by RT-PCR in the rodent gastrointestinal mucosa (137, 366). Wu and colleagues (366) also assessed expression of taste receptors in the gastrointestinal tract, however they only detected T2R bitter taste receptor transcripts and found no evidence for T1R expression in duodenal mucosa. As the T1R3 receptor had not been identified at the time these findings related only to assays using primers for T1R1 and T1R2. The negative result for T1R2 expression contrasts with that obtained in the current study and a subsequent study by Dyer and colleagues

(81), which showed amplification of T1R2 and T1R3 receptor transcripts from the intestinal mucosa. These positive findings for T1R expression may reflect differences in the sensitivities of the respective RT-PCR assays to detect expression of low abundance transcripts, such as T1R2 in whole mucosal samples. The current study has extended these findings and has provided the first RT-PCR evidence of specific TRPM5 expression in the intestinal mucosa.

The use of real time RT-PCR in this study provided new information on the relative expression levels of taste signal molecules. T1R2 was found to be the least abundant taste signal transcript in both tongue and intestinal samples – a predicted outcome based on the sweet-specific role of this receptor. The three taste modalities detected via GPRC signalling are detected by taste cells that are individually tuned to a single modality (377), such that T2R bitter and T1R sweet or umami taste receptors are expressed in mutually exclusive taste cell populations (1, 237). Taste molecules $G\alpha_{gust}$ and TRPM5 are involved in transduction of all three taste modalities (364, 377) and are correspondingly expressed in all three taste receptor cell populations. The T1R3 receptor is found in both sweet and umami sensing cells while T1R2 is expressed only in sweet sensing cells. A low abundance of T1R2 transcript levels in the tongue relates directly to expression in a specific, but small population of taste cells in the lingual epithelium. The low levels of T1R2 transcript in the gastrointestinal tract are consistent with this population characteristic and support the hypothesis that coding of sweet signals in the intestine occurs in the same manner as the tongue.

Direct comparison of taste molecule transcript levels of the tongue and gastrointestinal mucosa in this study are difficult to meaningfully interpret owing to differences in the tissue sampling process for each. Lingual epithelial samples were obtained from papillae areas of taste bud (and taste cell) concentration, whereas mucosal scrapings were harvested over a large tissue area and are likely to contain fewer solitary taste cells. However relative expression levels of taste molecules were compared between tissue types, with notable differences. $G\alpha_{gust}$ expression in the tongue was the most abundant of the taste transcripts while

TRPM5 levels were comparatively low. However TRPM5 was generally the most abundant taste molecule transcript in gastrointestinal samples. These differences in expression may reflect differences in taste signal transduction between the tongue and the gastrointestinal tract. The gastrointestinal tract also expresses other taste Gα-subunits, such as $G\alpha_{transducin}$ (366) and other candidate Gα-subunits which may functionally interact with taste receptors (250) and could subserve the role of $G\alpha_{gust}$. It is possible that gastrointestinal taste transduction involves taste pathways that differ from the tongue, and in which other Gα-subtypes and/or TRPM5 are more important functionally or in which TRPM5 is expressed in additional cell types. Expression profiling of individual cells from the lingual and gastrointestinal epithelium would be required to determine such differences in transduction pathways.

Real time RT-PCR was also used to investigate expression of taste molecules along the gastrointestinal tract to identify potential regions where taste detection of carbohydrate may be functionally important. T1R2, T1R3, $G\alpha_{gust}$ and TRPM5 transcript levels were compared in tissue samples from different regions of the upper gastrointestinal tract from the distal esophagus through to intestinal ileum. The distal esophagus was assayed as a negative control in these experiments as a potential non-chemosensory region of the gastrointestinal tract. There was no evidence for expression of T1R2, $G\alpha_{gust}$ or TRPM5 in the esophageal mucosa as expected, however low levels of T1R3 transcript were detected. In the absence of other key taste molecules it would seem that T1R3 is not engaged in taste transduction in the esophagus, at minimum, it would not function as a carbohydrate detector without T1R2. It is possible that T1R3 may be involved in the sensing of refluxate or ingested amino acids in the distal esophagus, although this hypothesis would require further investigation.

Interestingly the expression of the sweet taste receptor T1R2 was detected only in samples from the small intestine, and was absent from gastric samples. This suggests that sweet taste transduction is confined to the small intestine. The T1R3 receptor, although present in lower levels in the gastric mucosa, was

expressed at significantly higher levels in the mucosa of the proximal intestine. This specific expression pattern of T1R2 and T1R3 suggests that the small intestinal mucosa is the primary site of sweet taste transduction by the heterodimeric sweet taste receptor along the gastrointestinal tract.

Taste molecules other than T1R2 were expressed in the gastric mucosa but are unlikely to form part of a functional carbohydrate sensing pathway. As the T1R3 receptor acts as an umami receptor in heterodimeric form with T1R1, the stomach may be an important site for taste detection of proteins, however this possibility was not explored further as these studies focussed on carbohydrate detection. Transcript levels of taste molecules in the gastric mucosa were generally low, with the exception of $G\alpha_{gust}$ and TRPM5, which were expressed at peak gastrointestinal levels in the antrum. The presence of $G\alpha_{gust}$ in the rodent antrum has previously been noted (137, 366) and shown to be confined to solitary gastric 'taste' cells. In the absence of significant T1R1 expression the high transcript levels of $G\alpha_{gust}$ and TRPM5 in the antrum suggest they are likely to be coupled to other taste receptors such as T2R bitter receptors. Although not investigated in the present study T2R receptors have been previously reported in the antrum (366) and the sensing of bitter in this region may be an important ability in emetic species. On the tongue bitter receptors play an important role in discouraging the consumption of potentially harmful compounds but if gustatory screening fails and ingestion occurs, detection in the stomach may provide a key trigger for emesis in emetic species, thus limiting access to the absorptive surface of the intestine. Alternatively, activation of bitter sensing pathways in non-emetic rodents may lead to activation of compensatory mechanisms such as excess mucous secretion.

A subset of taste molecules displayed region specific expression within the small intestine. T1R2 transcript levels were significantly higher in the jejunum than in duodenum or ileum. The low expression levels in the ileum and duodenum reinforces the view that the jejunum is the predominant site of T1R2 expression and carbohydrate detection in mice. In terms of gastric motility glucose-induced feedback has been

unequivocally shown to be initiated by glucose exposure in the proximal intestine (218, 274, 354) whereas glucose restricted to the ileum either does not appear to induce reflexes such as delayed gastric emptying (360) or does so to a limited extent (188). These functional observations of glucose-induced feedback for gastric emptying are therefore consistent with T1R2 expression profiles in the gastrointestinal tract in the current study. However it should be noted that such a sensing mechanism may be feeding into many and differing pathways along the small intestine, including into the enteric nervous system.

In contrast to T1R2, $G\alpha_{gust}$ transcript levels were expressed at highest levels in the ileum. $G\alpha_{gust}$ expression has been described throughout the intestinal tract with immunoreactive cells reported in the colon (137) indicating that expression does occur in the distal gut. $G\alpha_{gust}$ positive cells have also been reported in the other tissues such as the pancreas (135) and nasal cavity (92) and these findings have led to the view that $G\alpha_{gust}$ may be a molecular component common to many chemosensory cell types. The expression patterns of T1R2 and $G\alpha_{gust}$ suggest that peak $G\alpha_{gust}$ expression in the ileum is unlikely to be linked primarily to carbohydrate-sensing, despite the limited expression of T1R2 in this region. The distal small intestine is capable of powerful reflex feedback in response to luminal fats, proteins and to a lesser extent, carbohydrates. This reflex feedback, termed the ileal brake (329), may involve $G\alpha_{gust}$ signaling in these primary responses to fats, protein and possibly irritants. However, it is important to note that mRNA transcript levels in gene quantification may not directly correlate with protein abundance, a fact demonstrated for many genes in yeast (114). Accordingly, it is important to assess protein expression in corresponding regions.

In this study protein expression was assessed using immunohistochemistry to localise taste molecules in sections of small intestine and identify primary sensor cells in the small intestine. The antibodies against $G\alpha_{gust}$, $G\gamma_{13}$, T1R3 and TRPM5 were used with varying effectiveness. T1R3, $G\alpha_{gust}$ and $G\gamma13$ antibodies were validated in control sections via their expression in spindle-shaped taste cells within taste buds. $G\alpha_{gust}$

and Gγ13 labelled taste cells in each of the fungiform, foliate and circumvallate papillae types - a distribution pattern that has been well established (27, 152, 208). In contrast, immunolabelling for T1R3 was rare or absent from the majority of taste cells in fungiform papillae, but frequent in foliate and circumvallate papillae taste buds. This topographical selectivity has been described in a previous study using *in situ* hybridisation, where less than 4% of fungiform taste cells showed evidence of T1R3 expression (298), while probe hybridization occurred in around 30% of foliate and circumvallate taste cells. These results serve to validate target recognition of T1R3, $G\alpha_{gust}$ and Gγ13 antibodies in taste cells in the lingual epithelium, and for subsequent investigations in gastrointestinal tissues. Unfortunately the TRPM5 antibody did not consistently label lingual taste cells indicating that this antibody was not an appropriate immunological tool for investigation of TRPM5 expression in gastrointestinal tissues and so no conclusions can be made from any findings.

Höfer and colleagues (137) were the first to demonstrate $G\alpha_{gust}$ immunoreactivity in individual epithelial cells within the gastrointestinal mucosa. These cells were identified in the gastric cardia and duodenum of rats and identified further as brush cells based on immunolabelling for cytoskeletal markers and morphometry. The current investigation has extended these findings to mice and has identified solitary $G\alpha_{gust}$ immunopositive cells in the villous epithelium of the small intestine. The expression of the taste trimeric G-protein, $G\gamma_{13}$, and T1R3 was also identified in epithelial cells of similar distribution, villi location and morphology to those immunopositive for $G\alpha_{gust}$. These results suggest that the taste molecules expressed in the intestinal mucosa detected with RT-PCR are translated into taste proteins that appear to have a specific distribution. However all taste molecule antibodies were raised in the same species and attempts to circumvent technical issues of their use in multi-label assays were not successful in the laboratory. As a consequence, it was not possible to confirm whether these three taste molecule proteins were expressed in the same cells. Confirmation of co-expression would provide strong support for a complete taste-like transduction pathway operating within individual intestinal epithelial cells. Despite the likelihood of these

$G\alpha_{gust}$, $G\gamma_{13}$, and T1R3 epithelial cell populations possessing chemosensory abilities, at this stage it is not possible to determine if they are intrinsically capable of sensing sweet or carbohydrates due to a lack of information on whether T1R2 protein is co-expressed.

The presence of taste molecule proteins in intestinal epithelial cells suggests these cells are primary candidates as sense cells in the anatomical model of nutrient detection by the epithelium rather than by sensory nerves. Detection of luminal nutrients by such sense cells could result in the release of mediators, which through paracrine actions may activate vagal afferent fibres in the mucosa. Vagal afferents themselves may be directly chemosensitive, although probably not using a taste transduction mechanism as immunohistochemistry for taste molecule proteins failed to show any immunopositive fibres in the mucosa. Our laboratory has further demonstrated that taste molecules are not expressed by vagal afferents, as RT-PCR failed to show amplification of taste molecule transcripts in whole nodose ganglia (258). Consequently, nutrient detection by intestinal taste cells could only activate vagal afferents through release of mediators from the epithelium. Although this does not preclude the possibility that glucose may directly influence afferent terminals through other mechanisms such as one coulpling glucose metabolism to cellular excitability such as in the pancreatic β-cell.

Interestingly, neuronal cell bodies identified by PGP9.5 labelling in the myenteric plexus were immunopositive for T1R3, $G\alpha_{gust}$ and $G\gamma_{13}$ in mice. There is evidence that intrinsic primary afferents directly respond to nutrients, and enteric neurons have been shown to be activated by glucose infusion in the duodenum and jejunum of rats (303). Investigations into the mechanisms of glucose sensing in enteric neurons in the guinea pig ileum have implicated K_{ATP} channels in the excitation of glucose responsive neurons (195) suggesting a mechanism similar to that in pancreatic β-cells operates in these cells. However this does not exclude the possibility that taste transduction pathways subserve direct nutrient sensing in intrinsic primary afferents. A high proportion of myenteric neurons appeared to contain immunolabel for

$G\alpha_{gust}$, and $G\gamma_{13}$, in contrast a lower number seemed to be T1R3 positive. This may suggest that only a subset of these neurons may be directly sweet or umami/glutamate sensing. The large proportion of myenteric neurons containing $G\alpha_{gust}$, and $G\gamma_{13}$, may indicate a different functioning mechanism such as to signal irritants or noxious substances through a bitter-like pathway and so consequently these proteins may be widely expressed within the enteric system. The expression of taste signal molecules in enteric neurons was not investigated further in these studies.

The investigations in this chapter have confirmed that taste molecules T1R2, T1R3, $G\alpha_{gust}$, $G\gamma_{13}$ and TRPM5 are specifically expressed in the intestinal mucosa in mice. Importantly expression of the sweet receptor T1R2 was shown to be confined to the small intestine and its higher level expression in proximal regions coincides with regions most active in carbohydrate absorption and generation of carbohydrate-induced reflex feedback. These results strongly indicate that a taste transduction pathway operates in the intestinal mucosa and may represent the molecular mechanism for luminal nutrient detection and subsequent triggering of reflex nutrient feedback via vagal pathways. The expression of taste molecule proteins in solitary epithelial cells implicates these cells as one type of primary sense cells of the gut. The identity and signalling capability of these taste cells involved in transducing luminal nutrients into nutrient signals requires further investigation, and is the subject of studies in the next chapter.